Addis Ababa University

Addis Ababa Institute of Technology

School of Electrical and Computer Engineering

Electromagnetic Radiation from Cable Harnesses on board Addis Ababa LRT

by

Zenawi Gebremichael

Advisor

Dr.-Ing. Getahun Mekuria

A thesis submitted to Addis Ababa University, Institute of Technology,
in partial fulfillment of the requirements for the Degree of Master of Science
in Electrical Engineering (Railway)

March 2016

Addis Ababa, Ethiopia

Addis Ababa University

Addis Ababa Institute of Technology

School of Electrical and Computer Engineering

Electromagnetic Radiation from Cable Harnesses on board Addis Ababa LRT

by

Zenawi Gebremichael

Approved by Board of Examiners

_____	_____	_____
Chairman, Department of Graduate Committee	Signature	Date
Dr.-Ing. Getahun Mekuria	_____	_____
Advisor	Signature	Date
_____	_____	_____
Internal Examiner	Signature	Date
_____	_____	_____
External Examiner	Signature	Date

Declaration

I, the undersigned, declare that this thesis is my original work, has not been submitted for a degree in this or any other universities, and all sources of materials used for the thesis have been fully acknowledged.

Zenawi Gebremichael	_____
Name	Signature
Addis Ababa, Ethiopia	March 2016
Place	Date of Submission

This thesis has been submitted with my approval as a university advisor.

Dr.-Ing. Getahun Mekuria	_____
Advisor's Name	Signature

Abstract

Electromagnetic Compatibility (EMC) is becoming the main concern of many industries. One aspect of EMC is limited Electromagnetic (EM) radiation from the source. In order for a given device, equipment or system not to cause Electromagnetic Interference (EMI), its radiation level must not exceed some regulatory limits accepted worldwide. This thesis researches electromagnetic radiation from cable harnesses on board Light Rail Transit (LRT) trams. Main target of the research is to compute high-frequency (HF) and low-frequency (LF) Electromagnetic Field (EMF) inside and outside the LRT tramcar and assess them against known standard limits. HF and LF fields have different nature in generating interference to a system. As a result, separate consideration of these fields was important.

Radiation level mainly depends on physical and electrical parameters of a given structure. To adhere to this basic principle, the study was conducted by collecting data about electrical value and geometrical positioning of cables on board Addis Ababa (AA) LRT trams. After collecting all relevant data, equivalent three-dimensional (3D) model was developed for electromagnetic simulation with the help of software. CST Studio Suite is mainly used for numerical computation of electric and magnetic fields in both LF and HF ranges.

The results obtained from software simulations were compared with standard regulatory limits. The limits are taken from International Commission on Non-Ionizing Radiation Protection (ICNIRP) for static magnetic fields, and Institute of Electrical and Electronics Engineers (IEEE) for static electric fields. IEEE sets 5 kV/m as exposure limit for *general public* and 20 kV/m for *controlled environment*. The ICNIRP limits on static magnetic fields have many varieties depending on the exposure characteristic (ceiling value, continuous exposure, and medical device). For Radio Frequency Interference (RFI), regulatory limits of Federal Communications Commission (FCC) are adopted.

Field distributions inside and near the tramcar vary spatially. In this thesis, more focus was given to internal floor of the tramcar and outside levels of the track. On smaller portion of the floor, near the cab side, static magnetic field distribution exceeding the limit for medical devices (0.5 mT) was observed; it reached 12 mT. However, the place with such phenomenon was very limited, and the other exposure characteristics (ceiling value and continuous exposure) were

never exceeded around the floor. Static electric field distribution around the floor of the tramcar was far below the corresponding regulatory limit, too. 5 kV/m was taken as assessment limit, and all field values were below it. Coming to RF EM radiation, the limits varied over subrange of the frequencies. EM simulation of a structural model was conducted, and the radiation levels were below the limits in both vertical and horizontal polarizations.

Key words: Electromagnetic Compatibility, Electromagnetic Interference, Radio Frequency Interferences, Radiated Emission, differential-mode current, common-mode current.

Acknowledgement

My first thank goes to my advisor, Dr.-Ing. Getahun Mekuria. He has greatly helped me under every aspect of this thesis work. I would also like to acknowledge all the staffs of the School of Electrical and Computer Engineering at Addis Ababa Institute of Technology (AAiT) for providing me all helpful materials and advices. Finally, I would like to thank all of my friends and families for their persistent support during my thesis work.

Contents

List of Figures

List of Tables

ACRONYMS

AA	Addis Ababa
AC	Alternating Current
ACGIH	American Conference of Governmental Industrial Hygienists
CISPR	International Special Committee on Radio Interference
CM	Common Mode
DC	Direct Current
DM	Differential Mode
ELF	Extremely Low frequency
EM	Electromagnetic
EMC	Electromagnetic Compatibility
EMF	Electromagnetic Field
EMI	Electromagnetic Interference
ERC	Ethiopian Railway Corporation
FCC	Federal Communications Commission
FIT	Finite Integration Technique
HF	High Frequency
ICNIRP	International Commission on Non-Ionizing Radiation Protection
IEEE	Institute of Electrical and Electronics Engineers
IGBT	Insulated Gate Bipolar Transistor
ITE	Information Technology Equipment
LF	Low Frequency
LISN	Line Impedance Stabilization Network
LRT	Light Rail Transit
MI	Modulation Index
MPE	Maximum Permissible Exposure
NRPB	National Radiological Protection Board
OCS	Overhead Contact System
PWM	Pulse Width Modulation

RF	Radio Frequency
RFI	Radio Frequency Interference
VVVF	Variable Voltage Variable Frequency
WHO	World Health Organization

Chapter 1

Introduction

1.1 Background

Modern railway systems make use of electrical and electronic devices on board trains. The new generation of LRT employs safety communication systems with onboard antennas in addition to high power electrical drives. Utilization of such equipment in proximity to each other, however, has its own drawback: a phenomenon known as Electromagnetic Interference (EMI) occurs [1]. EMI is attributed to the presence of EMFs surrounding any system inside which electrical activity happens.

Owing to the presence of those EMFs, any electrical or electronic device on board the train has a potential of causing or being susceptible to electromagnetic disturbances. The effect can range from commonplace to catastrophic. To address EMI problems, additional design requirements other than the functional performance of the system are imposed. FCC, for example, sets regulations for radio and wire communication in the United States.

In railway systems, pantograph-catenary interface is the major source of radiated emission [2]. Next to this, power electronic systems embedded in the train are responsible for emission of EM waves [3]. In addition to those unintentional radiations, the railway system makes use of intentional radiations for communication and signaling purposes [3], [4].

In this thesis, the possible EM pollutions inside the tram are studied taking the case of AA LRT. Modeling of on-board electrical and electronic devices is prepared from predefined geometry and known specifications. Those models are then analyzed for EMC with the help of EM simulators. Based on the analysis results, the devices are assessed for compliancy against basic regulatory limits. Identification of the main EMI sources helps in proposing better solutions of potential problems and devising mitigation techniques. Based on different literatures, shielding, grounding and filtering are the methods by which EM radiations can be suppressed.

1.2 Problem Statement

Onboard equipment of AA LRT has not been studied from stand point of EMC. This study gap may result in less knowledge of the potential EM disturbances in the intra system as well as between two different systems. Without good knowledge of EMC-compliancy, no one is capable of ensuring safe and reliable operation of the system. Radio communication systems inside the tram or in the surroundings are prominent victims of EM disturbances. Interaction of electrical circuits from each of the subsystem is known to results in EMI. In order to verify that onboard equipment meets the standard EMC requirements, implementation of EM analysis inside and outside the tram is required.

1.3 Research Objectives

The main objective of this work is to analyze EMI problems inside and outside running LRT trams. It specifically aims at the following:

- Analyzing static EMFs emanating from on-tram power cables
- Investigating RFIs resulting from HF common-mode (CM) currents
- Assessing whether the results comply with the standard regulatory limits

1.4 Methodology

Various procedural tasks were followed by the author in order to achieve the objective of the research. Here below is a list of the basic methods that are employed:

- **Preliminary Study**: This included overviews of previous works on EMI analysis of railway systems with emphasis on equipment on board LRT trams. Such equipment consists of electrical and electronic devices mounted on the tram. By reviewing similar works and papers, the author is equipped with the basic knowledge in EM characteristics of the systems under study.
- **Data Collection**: The procedural task next to literature reviewing was collection of data from Ethiopian Railway Corporation (ERC). Specifications of on-tram equipment, which are relevant to the study, are requested. This helped to establish the characteristic model

of equipment on board LRT tram. Once the model is developed using the proper software tools, analysis of the system is performed.

- **Software Modeling and Simulation**: Utilization of software greatly helps to overcome the difficulties which would be confronted while conducting practical analysis. In this thesis, hybrid simulation softwares are employed among which CST Studio Suite is the most used one. Using these softwares, models are developed for equipment specifications collected from ERC. Figure 3.7 illustrates the steps followed to conduct numerical computation with software tools.
- **Analysis of the Result**: The results obtained from software simulations are helpful in assessing the real onboard systems for EMC-compliancy. The results are compared with standard EMC requirements.

1.5 Related Works

Many studies on railway electromagnetic interferences have been carried out. They had their own methodology and approach to fulfill the required objectives. EMIs inside and outside railway trams have been studied and appropriate mitigation techniques proposed. There also existed studies on electromagnetic problems out of railway systems. They greatly help to bring the techniques to railway domain. Among the studies which made noticeable contributions are the following.

- In the work of [5] were presented modeling and simulation for computation of LF electromagnetic field radiated by high-voltage lines and selection of analytical models that interpret the electric and magnetic fields as a function of distance to the target object. The impact of electromagnetic pollutions from human health perspectives was also studied. *Modeling of magnetic field radiated by a three phase line*, which is developed in [5], can be applied for magnetic field estimation of onboard LRT cables with some modification. However, magnetic field emissions from onboard power cables are expected to be relatively small in magnitude as the three lines in power cables are closer to each other than three phase overhead transmission lines.
- Conducted EMI generated by a Pulse Width Modulation (PWM) inverter-fed induction motor drive system and overvoltages occurring at the motor terminals are analyzed in [6].

The induction motor HF equivalent circuit is extracted using a finite element analyses (Maxwell 3D software). The equivalent circuits of interconnecting cable and inverter are then connected to it to analyze the terminal overvoltage.

- Paper [3] establishes measurements abroad and near the moving train to characterize magnetic fields induced by embedded components of the electric traction system. HF problems caused by equipment mounted onboard of trams are analyzed.
- Thesis [7] proposes some solutions including adjustment of the rise and fall times of voltage pulse in order to mitigate EMC problems in vehicle PWM controlled loads. Fast rise and fall times of digital pulses are the primary contributors to HF spectral content of electrical signals. The higher the frequency of the signal to be passed through the coupling path, the more efficient the coupling path is. This efficiency can be reduced by just slowing the rise and fall times of digital signals, thereby reducing the HF spectral content. However, excessive slowing of the rise and fall times of digital signals should be avoided because it leads to digital circuitry malfunctions.
- Another work, [8], mainly deals with prediction of radiated emissions from power cable between converter and motor. This paper develops a software model for simulation of radio-frequency radiated emissions from the power cables. In order to calculate radiated emission from three phase cable, knowledge of the CM current is necessary. Because it is CM current that greatly contributes to radiation emission, the effect of LF functional currents is negligible. CM current estimation is presented in the work of [9].
- New experimental methods to characterize EM noise on board the train are presented by [10]. It tested two approaches to evaluate the EM noise which can affect onboard telecommunication systems: the time domain and the frequency domain measurement techniques. The time domain measurement method is well appropriate to collect the whole spectrum of time transient emissions but requires post processing. Measurements in frequency domain are, however, easier to carry out and suitable for standardization.

1.6 Thesis Organization

This thesis is organized into five chapters. Each chapter gives detailed explanation of the relevant topic. The first chapter provides with introduction, objective and methodology of the research.

The second chapter consists of general introduction and theoretical background about EMC. The well-known analytical formulae of EMC/EMI and the standard regulatory limits are covered in this chapter.

In chapter three, EMI modeling of onboard LRT equipment is developed. Both LF and HF electromagnetic problems that may appear on board the tram are discussed and the most important components responsible for generation of such fields identified.

The fourth chapter is dedicated for software simulations of EMI around cable harnesses. The possible EMI sources with developed models are simulated and compared with standard regulatory limits.

Chapter five includes conclusions and recommendations. Implications of the results and future works are stated in this chapter.

Chapter 2

Electromagnetic Field and EMI

2.1 Introduction

Throughout history, many disturbances of electromagnetic nature have been observed. As a result, various electrical and electronic devices were prone to those disturbances. Among the well-known sources of electromagnetic emissions are lightning, relays, electric machines, high-voltage power transmission lines, radio and radar transmitters, and digital electronic devices. Utilization of pulses to represent a binary number, 0 (off) or 1 (on), needs limited transition time of the pulse from off to on and vice versa. The faster the transition times, the wider the range of frequencies generated [1]. All these are the factors for unwanted interferences.

EMI affects healthy functioning of a device, equipment or a system. A system is said to be electromagnetically compatible if it functions in its electromagnetic environment without introducing intolerable electromagnetic disturbances in that environment [11]. As stated by [1]: "A system is electromagnetically compatible with its environment if it satisfies three criteria:

1. It does not cause interference with other systems.
2. It is not susceptible to emissions from other systems.
3. It does not cause interference with itself."

Interference occurs when EM energy generated by a source is transmitted via a coupling path and begins to affect a receptor. Figure 2.1 shows the three elements of EMC problems: source (emitter), coupling path and a receptor (receiver) [1].

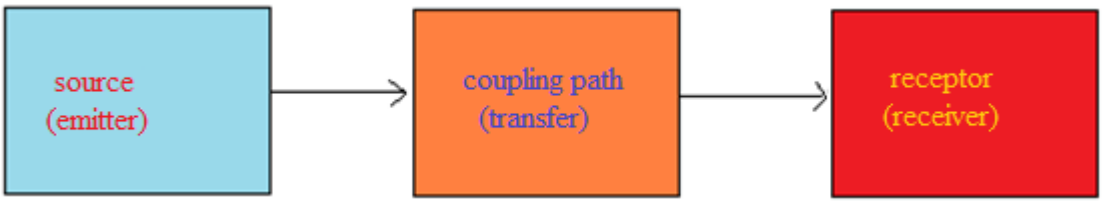

Figure 2.1. Basic aspects of EMC problem [1].

There are three ways to prevent interference [1]:

1. Suppress the emission at its source.
2. Make the coupling path as inefficient as possible.
3. Make the receptor less susceptible to the emission.

It is easier to reduce the coupling by working from left to right in Fig. 2.1. Suppression of EM emissions at their source is more effective than protection of the receptors from the emission [1].

EMFs can be roughly classified into two based on their frequency: LF and HF EMF. Extremely Low Frequency (ELF) fields are non-ionizing radiation contained in the range of LF signals. According to United States government agencies, frequency range of ELF EMFs is between 0 and 300 Hz. They are related to static fields or 60 Hz electricity. Prominent sources of ELF EMFs exist, including power lines, substations, appliances, electric motors and generators. Radio-frequency (RF) signals, on the other hand, are unique elements of HF signals whose frequency extends from 9 kHz to 3000 GHz. Those two forms of EM energy, ELF and RF EMFs, have inevitable relevance to EMI and are explained in Section 2.3 and 2.4 respectively.

2.2 Electromagnetic Coupling

EMI occurs only when the emitter and receiver pictured in Fig. 2.1 interact through the coupling medium. There are a number of ways for the emissions to be coupled into the receiver. The coupling types are classified into four based on their transmission mode [12]:

1. Galvanic coupling
2. Capacitive coupling
3. Inductive coupling
4. Radiative coupling

2.2.1 Galvanic Coupling (Common Impedance)

When current flows through the shared conductor, CM voltage noise is generated. Figure 2.2 illustrates how two devices share the same conductor. The current drawn by one of the electrical devices in Fig. 2.2 causes a voltage drop in the common impedance, and this voltage drop causes a dip in the supply voltage of the other circuit [12].

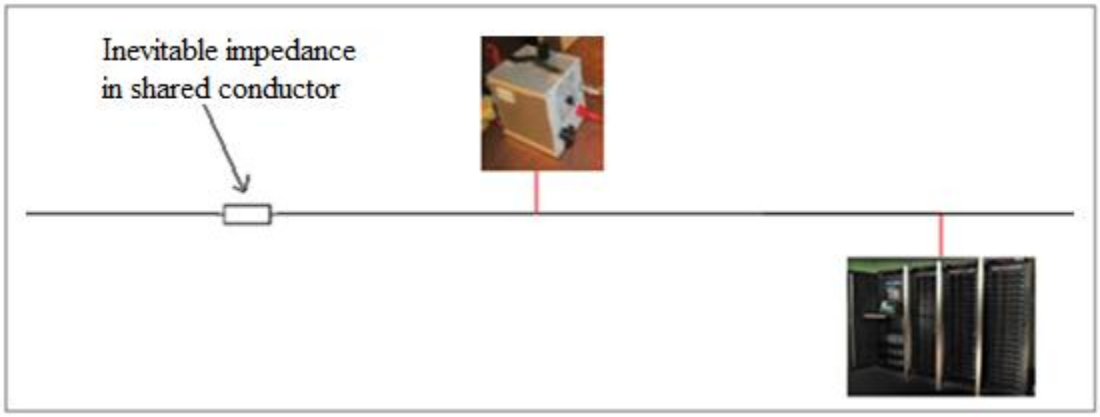

Figure 2.2. Galvanic coupling [Author].

Galvanic coupling between two electrical circuits can be reduced by the following methods [12]:

- ✓ Separate supplies for power circuits and low-level signal circuits
- ✓ Star connection to reduce the common impedance

2.2.2 Capacitive Coupling (Electric Coupling)

It is a coupling type that takes place when time varying electric field from one circuit injects noise current to the victim circuit via mutual capacitance (stray capacitance). This phenomenon comes to appear when a conductor placed close to another conductor or metallic sheet enclosing the cable is supplied with finite voltage difference.

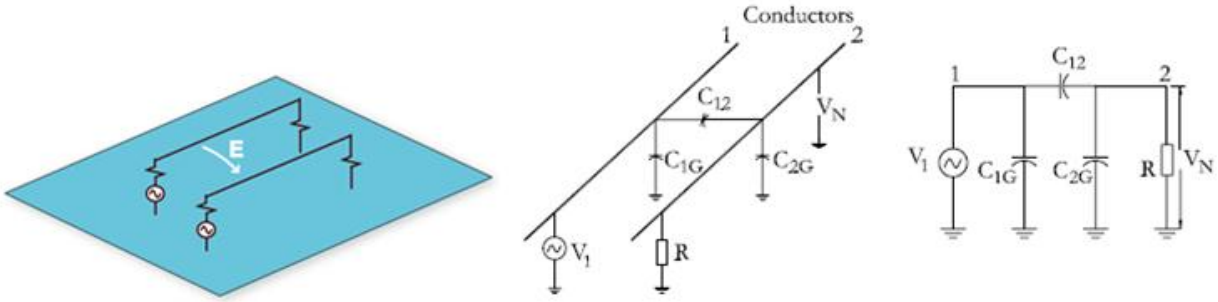

(a) (b) (c)

Figure 2.3. Capacitive coupling [7]. (a) Two circuits above a plane. (b) Physical representation. (c) Equivalent circuit.

As shown in Fig. 2.3b, presence of a voltage, V_1, in the source circuit causes the receptor circuit to develop a noise voltage, V_N. V_N is expressed in terms of V_1 as follows [7]:

$$V_{N=}\frac{j\omega\left[\frac{C_{12}}{C_{12}+C_{2G}}\right]}{j\omega+\frac{1}{R(C_{12}+C_{2G})}}V_1 \tag{2.1}$$

Where,

C_{12} - stray capacitance between the two conductors

C_{2G} - capacitance between conductor and ground

R- Resistance between the receptor circuit and ground.

For resistance *R* with lower impedance, Eq. (2.1) is reduced to the following equation:

$$V_N = j\omega RC_{12}V_1$$

$$= j2\pi fRC_{12}V_1 \tag{2.2}$$

As shown in Eq. (2.2), the main parameters that greatly affect the noise voltage are frequency, resistance and stray capacitance. Two methods are practically applicable to reduce capacitive coupling [7]:

- ✓ Decreasing resistance by operating the receiver circuit at low resistance level
- ✓ Decreasing stray capacitance by changing orientation of the conductors, shielding and moving the conductors farther apart.

An example of capacitive coupling between two conductors of the same radius can be expressed in terms of per-unit-length parameters as given in Eq. (2.3).

$$\frac{C}{l}=\frac{\pi\varepsilon}{\ln\left(\frac{D}{d}+\sqrt{\left(\frac{D}{d}\right)^2-1}\right)} \tag{2.3}$$

D is the distance between the two conductors and *d* the diameter of each conductor.

2.2.3 Inductive Coupling (Magnetic Coupling)

It is a coupling type that takes place when time varying magnetic field from one circuit induces noise voltage in the victim circuit via mutual inductance.

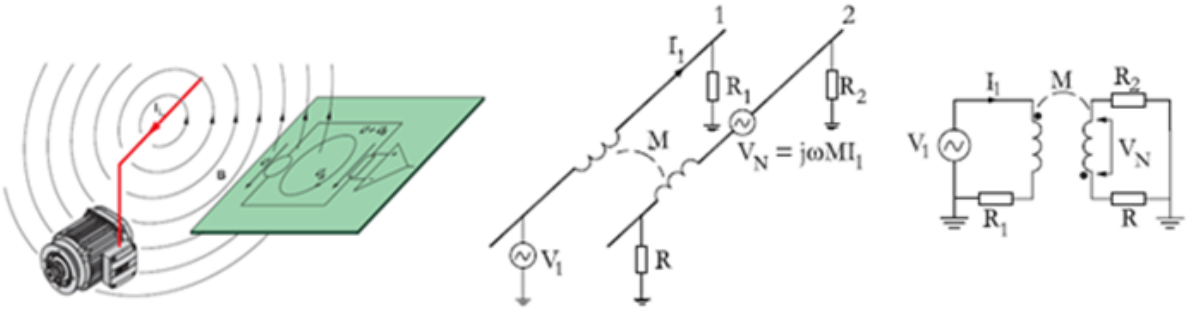

(a) (b) (c)

Figure 2.4. Inductive coupling [7], [12]. (a) Practical example. (b) Physical representation. (c) Equivalent circuit.

The noise voltage, V_N, is expressed as follows:

$$V_N = -\frac{d}{dt}\int_A \mathbf{B}.\mathbf{dA} \tag{2.4}$$

B is the flux density and **A** the loop area. The expression for the noise voltage reduces to Eq. (2.5) when the loop area is stationary relative to sinusoidally varying flux density [7].

$$V_N = j\omega BA\cos\theta$$

$$= j\omega MI_1 = M\frac{dI_1}{dt} \tag{2.5}$$

Where,

θ - the angle between the loop area and the magnetic flux density

I_1 - the current in the source circuit

M - the mutual inductance between the receptor and source circuit

The coupling between the two circuits is directly proportional to the frequency, ω, the magnetic flux density, B, the loop area, A, and the angle between A and B, θ. The frequency of the noise voltage cannot be changed and hence the parameters that can be modified in order to reduce the noise voltage are the remaining ones: A, B and the angle between them, θ [7].

- ✓ Flux density reduction by physical separation of the circuits and twisting the wires.
- ✓ Loop area reduction by placing the conductor close to the ground plane.
- ✓ Placement of the source and receiver circuits in such a way that the $\cos\theta$ term is decreased.

2.2.4 Radiative Coupling

Beyond some region, the electric and magnetic fields of a source combines and travel as EM waves. This region is the boundary for near field and far field radiation. When the travelling EM waves couple to any circuit, a voltage is induced in it.

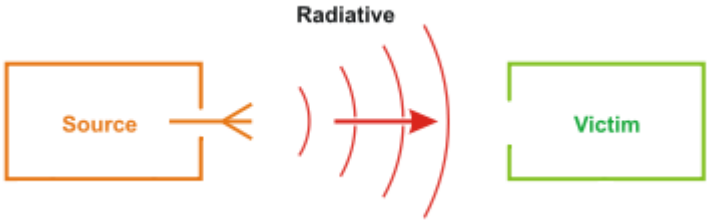

Figure 2.5. Radiative coupling between two devices.

2.3 Extremely Low Frequency EMF

ELF fields are those having frequencies from 0 Hz up to 300 Hz. In that frequency range, the electric and magnetic fields act independently of one another and are measured separately [13].

Electric fields are attributed to static or moving electric charges, whereas magnetic fields result from moving electric charges i.e current [13]. Hence if any point charge is in rest, only electric field is observed around it. If it is in motion, however, both electric and magnetic fields exist. Electric field results from static electric dipoles, too. Both electric and magnetic fields are highest close to the device that generates them and decrease with distance. Electric fields are easily shielded by common materials whereas magnetic fields are capable of penetrating all but ferromagnetic materials [13].

In macroscopic world, magnetic fields are observed resulting from a current running along a conductor, and electric fields from a voltage applied across two conductors (opposite charges accumulate on the two ends of the conductor). If a conductor is connected to power socket, electric field is generated for the nominal voltage between the conductor and ground; but magnetic fields are not observed until current starts flowing through the conductor.

The basic elements from which models of complex wires can be derived are electric (Hertzian) dipole and magnetic dipole (current loop). The Hertzian dipole is an infinitesimal current element whose current is assumed to be the same at all points [1]. The magnetic dipole, on the

other hand, is a very small loop of current element. All kinds of fields emanating from these elements are discussed in detail in Section 2.4.2. The field types are categorized based on their variation as function of distance from the source and the frequency content they have. As pointed out in that section, electrostatic and induction fields are field types which predominantly appear in LF range.

Health effects of LF EMFs are the subject of ongoing research. There are, however, some confirmed experimental evidences that ELF electric and magnetic fields have some considerable impacts. The following lists ensure the effects of ELF EMFs:

- Possible associations between exposure to ELF magnetic fields and risk of cancer in children (leukemia and brain tumors) [14].
- Possibility of electric fields from transmission lines interfering with synchronous cardiac pacemakers.
- Short-term annoying field perception and painful spark discharges resulting from static electric fields [15].

Based on researches and studies, the World Health Organization (WHO) classified EMFs as the cause of some diseases. Owing to this fact, exposure standards have been developed internationally. The guidelines vary depending on the EMF frequency and type of the victim affected. The biological effects of time-varying fields, for example, are detectable at lower levels compared with that of static fields. Static and time-varying fields, as a result, have different guidelines. Coming to the victim-based classification, public exposure limits are more restrictive than occupational exposure limits.

There are some standard limits on ELF EMFs from health risk perspective. ICNIRP, IEEE, ACGIH and NRPB are the four main organizations that have set limits on these fields. Exposure limits on time-varying electric and magnetic fields (50/60Hz) are put in Table 2.1 in combination. Table 2.2 shows exposure limits on static magnetic fields. Maximum Permissible Exposure (MPE) limits on whole-body electric field exposure are given in Table 2.3 as function of frequency.

The guidelines developed by ICNIRP are widely recognized in several countries. The World Health Organization (WHO) and the European Union (E.U.) have adopted the limits of ICNIRP [16]. Thus, ICNIRP is preferred to be a guideline for assessing LF EMF pollutions in this thesis.

Table 2.1. Exposure limits of different agencies on time-varying ELF EMFs.

	NRPB-1993	*ACGIH-2000*	*ICNIRP-1998*	*IEEE 2002*
Occupational				
Electric field, kV/m	12	25	10	20
Magnetic field, mT	1.3	1.0	0.5	2.71
Public				
Electric field, kV/m	12	NA	5	5
Magnetic field, mT	1.3	NA	0.1	0.904

Guidelines for static electric and static magnetic fields have been issued separately in the following tables. Compared with time-varying EMFs, exposure limits on static fields are less restrictive as reasoned out previously.

Table 2.2. Exposure limits on static magnetic fields [17].

Exposure characteristics		Magnetic flux density(mT)
Occupational	Whole working day	200
	Ceiling value	2000
	Limbs	5000
General public	Continuous exposure	40
Medical devices		0.5

Table 2.3. IEEE electric field MPE limits [15].

Frequency, Hz	Exposure Limit, kV/m	
	Controlled Environment	General Public
< 1	≥ 20	≥ 5
$1 - 272[368]^a$	20	5
$272[368]^a - 3000$	$^{5440}/_{f}$	$^{1840}/_{f}$
> 3000	1.813	0.614

[a] 272 Hz for controlled environment; 368 Hz for general public

2.4 Radio Frequency EMF

As defined by FCC, the range of radio frequencies extends from 9 kHz to 3000 GHz [1]. A radio-frequency device is capable of emitting radio-frequency energy. DC motors and digital computers are among radio-frequency devices. The kind of interference caused by radio-frequency fields is termed as Radio Frequency Interference (RFI). RFIs are characterized by the following four categories (also shown in Fig. 2.6) with regard to their prevention method [1].

1. Conducted emissions
2. Radiated emissions
3. Conducted susceptibility
4. Radiated susceptibility

Conducted emissions are observed as transmitted noise voltage/current in a given system whereas radiated emissions generate EM noises around the free space medium. The second aspect, radiated emission, is the main concern in this thesis.

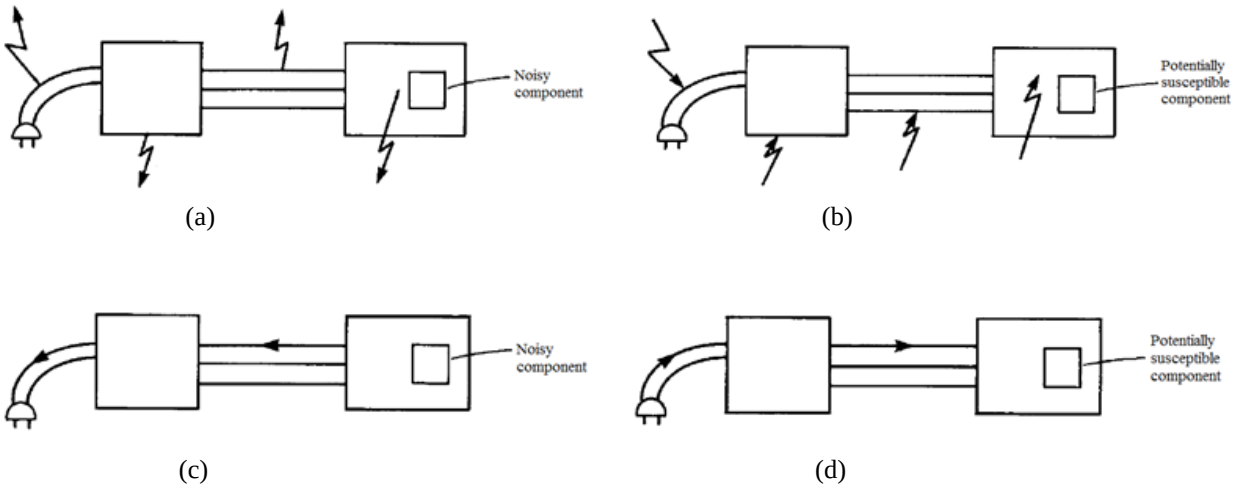

Figure 2.6. The four EMC problems [1]: (a) Radiated emissions. (b) Radiated susceptibility. (c) Conducted emissions. (d) Conducted susceptibility.

The components shown in Fig. 2.6 consist of one or more cables. These cables can emit and/or pick up electromagnetic energy. Longer cables have higher capability of causing EMI compared with shorter cables.

2.4.1 Conducted Emission

Conducted emissions are kind of electromagnetic interferences which manifest as current noises conducted out a given electrical system along its interconnecting cables. The source of emission in the system may be directly connected circuits or unrelated circuits coupling electromagnetically to the given system. Some conducted emissions have sufficient magnitude to cause direct interference whereas others have too small magnitude. The conductors act as 'accidental transmitting antenna', and the current running along them generates radiated electromagnetic field instead. Generally, the reduction of conducted emissions is simpler than reduction of radiated emissions [1].

Measurement of conducted emissions

Based on FCC and CISPR 22 rules, frequency range of limits on conducted emissions extends from 150 kHz to 30 MHz. [1]. Conducted emissions are measured with a line impedance stabilization network (LISN) inserted between the commercial power outlet and product's ac power cord [1]. AC power is sent to the product through the LISN. Spectrum analyzer is attached to LISN to measure conducted emission [1].

The LISN, which is shown in Fig. 2.7, has two advantages [1]:

- It delivers constant impedance to the product's power cord outlet over the frequency range of the conducted emission test (the 50 Ω resistor in Fig. 2.7 ensures this task).
- It blocks irrelevant emissions coming from external system, thereby avoiding contamination of the test data (the 1 mF capacitors and 50 mH inductors in Fig. 2.7 used for this purpose).

LISN is active only for frequency range lying in 150 kHz-30 MHz, and an AC power below that range simply passes without being detected. The LISN circuit is designed in such a way that over the measurement frequency range, the capacitors act as short circuits and the inductors as open circuits.

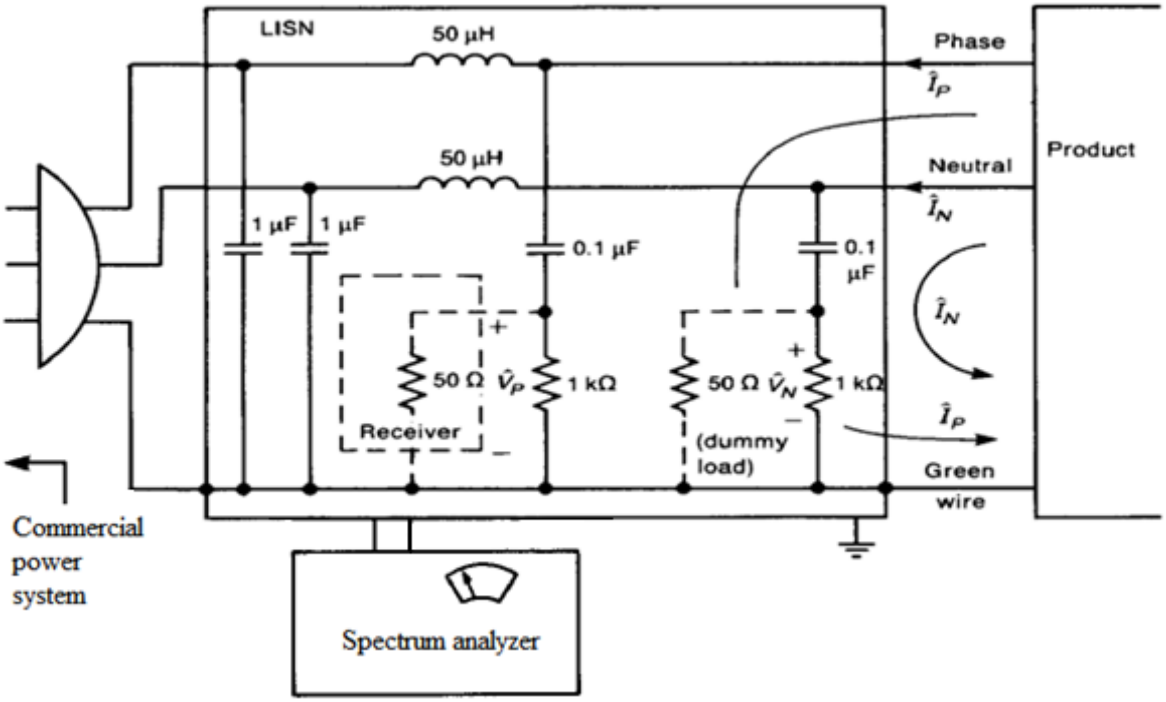

Figure 2.7. Illustration of the LISN circuit [1].

The phase-safety wire voltage and neutral-safety wire voltage, V_P and V_N, must be below the regulatory limit in conducted emission frequency range. Conducted emission currents are of greater interest than the voltages. The following equations express how the phase current I_P and the neutral current I_N are related to the measured voltages. These equations are obtained noting that the inductors in Fig. 2.7 act as open circuits, and hence I_P and I_N flow through the 50 Ω resistors, not branching off toward the inductors.

$$V_P = 50I_P \tag{2.6a}$$

$$V_N = 50I_N \tag{2.6b}$$

The emission currents expressed in Eq. (2.6) can be decomposed into differential-mode (DM) and common-mode (CM) component. DM current loops around the given circuit whereas CM current flows parallel through the two sides of the circuit (phase and neutral) and returns via the ground (green wire). Equation (2.8) shows how DM and CM currents are expressed in terms of I_P and I_N.

$$I_P = I_C + I_D \tag{2.7a}$$

$$I_N = I_C - I_D \tag{2.7b}$$

Solving the above equations, we get the following:

$$I_D = \frac{1}{2}(I_P - I_N) \tag{2.8a}$$

$$I_C = \frac{1}{2}(I_P + I_N) \tag{2.8b}$$

2.4.2 Radiated Emission

Frequency range of radiated emissions measurement is from 30 MHz to over 1 GHz. FCC set measurement distances to be 3 m for Class B products and 10 m for Class A products whereas for CISPR 22 (EN55022), the measurement distance is 10 m for both Class A and Class B products [1]. Figure 2.8 illustrates how radiated electric field of a product is measured in a semi anechoic chamber.

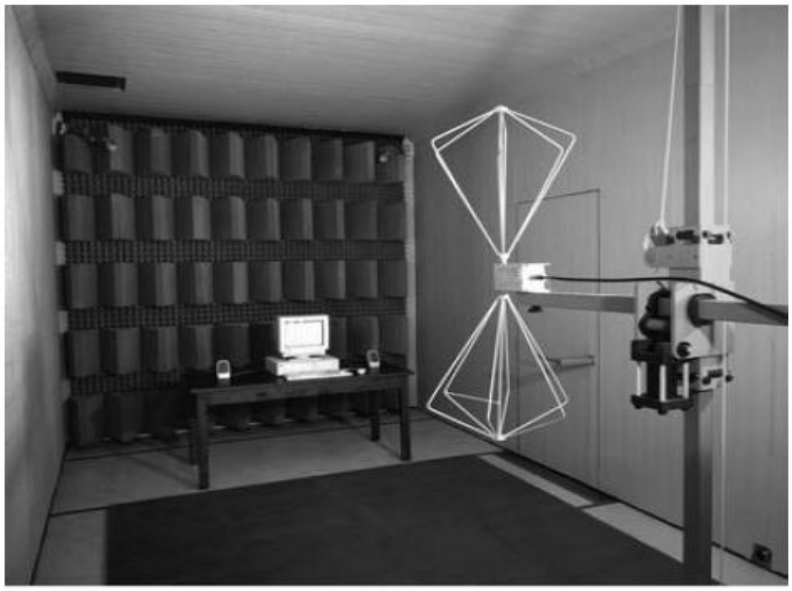

Figure 2.8. Illustration of a typical test of a device for its radiated emissions (courtesy of ETS-Lindgren, Inc.).

The field structure of the emissions in the near field of an emitter is more complicated than in the far field. The boundary between near field and far field is where the electric and magnetic fields combine to EM waves and travel as one entity. Near field calculations can't use simplifications

which are valid for far field. An example of the simplifications is inverse-distance rule. In the near field, there exist more terms like $1/r^2$ and $1/r^3$ that make the inverse-distance rule fail. Their effect vanishes only at a considerable distance.

It is imperative to consider the emission levels of both electric (Hertzian) dipole and magnetic dipole (current loop) since the simple models of wires can be derived from these elements. Electrically short elements are elements whose dimension is much smaller than the wavelength of the signal travelling through them ($< \frac{\lambda_0}{10}$). For electrically long elements, however, the signals levels at a given time vary along the length; and the emission level calculations get more complicated.

Elemental dipole antennas

Electric dipole and *magnetic dipole* are the most familiar antenna elements. They are so electrically short that the current distribution along the elements has the same magnitude and phase at a given time. One more interesting fact is that they are dual to each other. Here below is detailed explanation of those antennas along with mathematical equation of the corresponding radiation fields.

The electric (Hertzian) dipole: The Hertzian dipole is an infinitesimal current element with length *l* and phasor current $\hat{I}$. The current is assumed to be the same along the entire length both in magnitude and phase [1]. Figure 2.9 portrays a Hertzian Dipole in spherical coordinate system. The magnetic field intensity vector has the following components [18].

$$\hat{H}_r = 0 \tag{2.9a}$$

$$\hat{H}_\theta = 0 \tag{2.9b}$$

$$\hat{H}_\Phi = \frac{\hat{I}l}{4\pi}\beta_0^2 \sin\theta \left(j\frac{1}{\beta_0 r} + \frac{1}{\beta_0^2 r^2}\right) e^{-j\beta_0 r} \tag{2.9c}$$

The components of the electric field intensity vector are likewise stated as [18]

$$\hat{E}_r = 2\frac{\hat{I}l}{4\pi}\eta_0\beta_0^2 \cos\theta \left(\frac{1}{\beta_0^2 r^2} - j\frac{1}{\beta_0^3 r^3}\right) e^{-j\beta_0 r} \tag{2.10a}$$

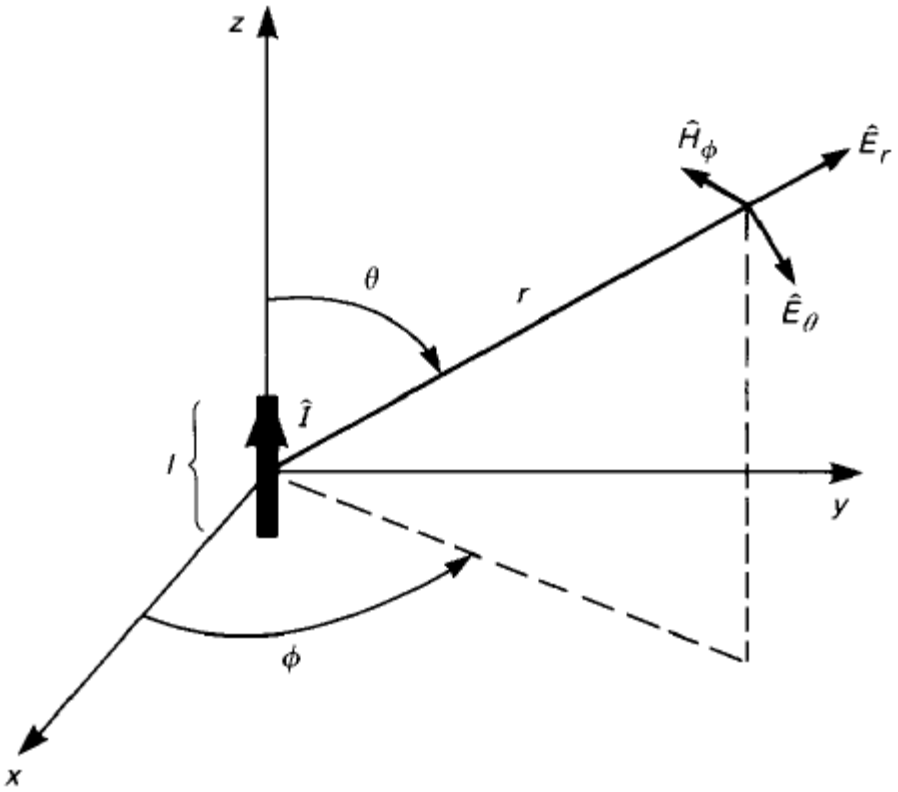

Figure 2.9. The Hertzian Dipole [1].

$$\hat{E}_\theta = \frac{\hat{I}l}{4\pi}\eta_0\beta_0^2 \sin\theta \left(j\frac{1}{\beta_0 r} + \frac{1}{\beta_0^2 r^2} - j\frac{1}{\beta_0^3 r^3}\right) e^{-j\beta_0 r} \tag{2.10b}$$

$$\hat{E}_\Phi = 0 \tag{2.10c}$$

where $\eta_0 = \sqrt{\mu_0/\varepsilon_0}$ is the intrinsic impedance in free space, and $\beta_0 = 2\pi/\lambda_0$.
Depending upon their variation as a function of distance, EMFs from a simple Hertzian dipole are grouped into three.

- The $1/r^3$-term, *electrostatic field*, surrounds the nearest zone of the dipole and dramatically diminishes as function of distance. Electrostatic field is essentially due to the accumulation of charges on the tip of the antenna (oscillating dipole). It is inversely proportional to the frequency.
- The $1/r^2$-term, *induction field*, extends little further than the electrostatic field but still diminishes as a function of distance. It is independent of frequency.

- The $1/r$-term, *radiation field*, extends more to farthest distance compared with the previous two fields. Power radiation from an antenna is fulfilled through this field type. Radiation field is directly proportional to the frequency. That is why it is more prevalent at high frequencies than at low frequencies.

In the near field of the antenna, the electrostatic and the induction fields dominate whereas in far field radiation fields dominate for their highest order term. Therefore, near fields mainly consist of electrostatic and induction fields whereas far fields are attributed to radiation fields. Unlike in radio communication systems, which deal with only far field region, much focus is given to all of these field types from EMC standpoint.

The three fields have equal magnitude at a distance of $r \cong \frac{1}{6}\lambda_0$ as shown in Fig. 2.10. This point is referred to as the boundary between the near field and the far field, but for other antenna types, it may vary and is not simply $\frac{1}{6}\lambda_0$.

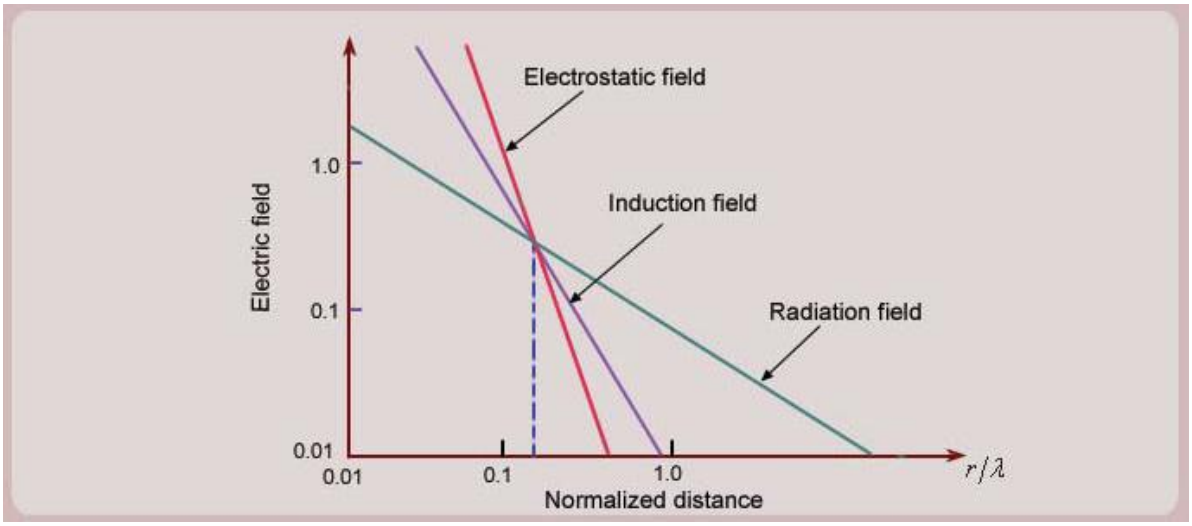

Figure 2.10. The three kinds of fields as function of distance.

For far field point, only the $1/r$-term is assumed. The field expressions in Eqs. (2.11) and (2.12) show far-field vectors.

$$\hat{\mathbf{E}}_{\text{far field}} = j\eta_0\beta_0 \frac{\hat{I}l}{4\pi}\sin\theta \ \frac{e^{-j\beta_0 r}}{r}\ \mathbf{a}_\theta$$

$$= j\frac{f\mu_0}{2}\hat{I}l\sin\theta\left\{\frac{e^{-j\left[2\pi\left(r/\lambda_0\right)\right]}}{r}\right\} \qquad (2.11)$$

$$\hat{\mathbf{H}}_{\text{far field}} = j\beta_0 \frac{\hat{I}l}{4\pi} \sin\theta \ \frac{e^{-j\beta_0 r}}{r} \ \mathbf{a}_\Phi$$

$$= j \frac{f\mu_0}{2\eta_0} \hat{I}l \sin\theta \left\{ \frac{e^{-j\left[2\pi\left(r/\lambda_0\right)\right]}}{r} \right\} \tag{2.12}$$

Where $\beta_0 = {}^{2\pi}/_{\lambda_0}$.

The time-domain fields are just the real part of the phasor fields multiplied by $e^{j\omega t}$ [1]:

$$\mathbf{E}_{\text{far field}} = Re\{\mathbf{E}_{\text{far field}} e^{j\omega t}\}$$

$$= -\frac{E_m}{r} sin\left[\omega\left(t - \frac{r}{v_0}\right)\right] \mathbf{a}_\theta \tag{2.13}$$

$$\mathbf{H}_{\text{far field}} = Re\{\mathbf{H}_{\text{far field}} \, e^{j\omega t}\}$$

$$= -\frac{E_m}{\eta_0 r} sin\left[\omega\left(t - \frac{r}{v_0}\right)\right] \mathbf{a}_\Phi \tag{2.14}$$

Where $E_m = \frac{\eta_0 \beta_0 \hat{I}l}{4\pi} \sin\theta$

$= \frac{f\mu_0}{2} \hat{I}l \sin\theta = 6.283 \times 10^{-7}\left(fl\hat{I}\right) \sin\theta$

The magnetic dipole (loop): The elemental magnetic dipole, which is dual to the elemental electric dipole, is a very small loop of radius b carrying a phasor current $\hat{I}$. In Fig. 2.11 is illustrated a magnetic dipole lying in the xy plane. The loop circumference is assumed to be electrically small, i.e, $2\pi b < \frac{\lambda_0}{10}$. The loop makes up magnetic dipole moment which is expressed in the following equation [18].

$$\hat{m} = \hat{I}\pi b^2 \text{ (in Am}^2\text{)} \tag{2.15}$$

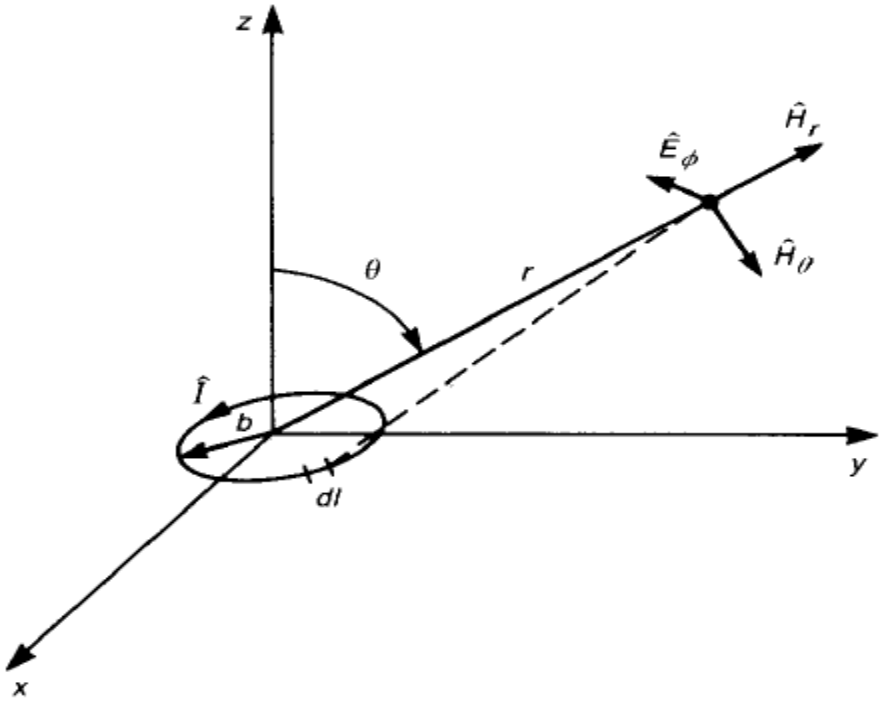

Figure 2.11. The magnetic dipole [1].

The electric fields of the magnetic dipole are,

$$\hat{E}_r = 0 \tag{2.16a}$$

$$\hat{E}_\theta = 0 \tag{2.16b}$$

$$\hat{E}_\Phi = -j\frac{\omega\mu_0\hat{m}\beta_0^2}{4\pi}\sin\theta\left(j\frac{1}{\beta_0 r}+\frac{1}{\beta_0^2 r^2}\right)e^{-j\beta_0 r} \tag{2.16c}$$

whereas the magnetic fields are stated as follows [18].

$$\hat{H}_r = j2\frac{\omega\mu_0\hat{m}\beta_0^2}{4\pi\eta_0}\cos\theta\left(\frac{1}{\beta_0^2 r^2}-j\frac{1}{\beta_0^3 r^3}\right)e^{-j\beta_0 r} \tag{2.17a}$$

$$\hat{H}_\theta = j\frac{\omega\mu_0\hat{m}\beta_0^2}{4\pi\eta_0}\sin\theta\left(j\frac{1}{\beta_0 r}+\frac{1}{\beta_0^2 r^2}-j\frac{1}{\beta_0^3 r^3}\right)e^{-j\beta_0 r} \tag{2.17b}$$

$$\hat{H}_\Phi = 0 \tag{2.17c}$$

The far field of the magnetic dipole was obtained by considering only the $1/r$-terms.

$$\hat{\mathbf{E}}_{\text{far field}} = \frac{\omega\mu_0\hat{m}\beta_0}{4\pi}\sin\theta\ \frac{e^{-j\beta_0 r}}{r}\ \mathbf{a}_\Phi$$

$$= \frac{\pi^2 f^2 \mu_0 \hat{I} b^2}{v_0}\sin\theta\left\{\frac{e^{-j\left[2\pi\left(r/\lambda_0\right)\right]}}{r}\right\} \tag{2.18}$$

$$\hat{\mathbf{H}}_{\text{far field}} = -\frac{\omega\mu_0\hat{m}\beta_0}{4\pi\eta_0}\sin\theta\ \frac{e^{-j\beta_0 r}}{r}\ \mathbf{a}_\theta$$

$$= \frac{\pi^2 f^2 \mu_0 \hat{I} b^2}{\eta_0 v_0}\sin\theta\left\{\frac{e^{-j\left[2\pi\left(r/\lambda_0\right)\right]}}{r}\right\} \tag{2.19}$$

As was done for the Hertzian (electric) dipole, the time-domain fields are obtained by multiplying the phasor fields by $e^{j\omega t}$ and extracting real part of the results.

2.5 EMC Requirements

In addition to their functional performances, electronic systems are required to satisfy basic EMC rules across the world. EMC requirements for RF devices are categorized into two classes [1]:

1. Those mandated by governmental agencies
2. Those imposed by the product manufacturer

The requirements mandated by governmental agencies are imposed in order to control the amount of electromagnetic emission that the product generates. Product manufacturers may also impose EMC requirements on their products to increase customer satisfaction. EMC requirements of all countries imposed by governmental agencies are divided into two classes: requirements for products marketed in the United States (USA) and requirements for products marketed outside the United States [1].

2.5.1 Requirements for Commercial Products Marketed in the United States

FCC is charged with the regulation of radio and wire communication in USA. According to FCC rules, digital device are divided into two: Class A and Class B. Class A digital devices are mainly employed in commercial, industrial, or business environment whereas Class B digital

devices are employed in residential environment. Class B limits are more restrictive than the Class A limits [1].

For conducted emission test, LISN is inserted into the unit's ac power cord and the frequency range is set to 150 kHz-30 MHz. In radiated emission test, on the other hand, radiated electric field of the product is measured either in a semi anechoic chamber or at an open-field test site [1]. The measurement must be done in both vertical and horizontal polarizations with respect to the ground plane, and the frequency range is from 30 MHz up to 40 GHz. But CISPR 22 requirement currently doesn't extend beyond 1 GHz. The following tables illustrate the conducted and radiated emission limits for Class A and Class B digital devices.

Table 2.4. FCC and CISPR 22 conducted emission limits for Class B digital devices.

Frequency(MHz)	μV QP (AV)	dBμV QP (AV)
0.15	1995 (631)	66 (56)
0.5	631(199.5)	56 (46)
0.5-5	631 (199.5)	56 (46)
5-30	1000(316)	60(50)

Table 2.5. FCC and CISPR 22 conducted emission limits for Class A digital devices.

Frequency(MHz)	μV QP (AV)	dBμV QP (AV)
0.15-0.5	8912.5 (1995)	79 (66)
0.5-30	4467 (1000)	73 (60)

Table 2.6. FCC radiated emission limits for Class B digital devices.

Frequency(MHz)	measured at 3 m	
	μV/m	dBμV/m
30-88	100	40
88-216	150	43.5
216-960	200	46
>960	500	54
>1 Ghz	500(AV)	54(AV)
	5000(PK)	74(PK)

Table 2.7. FCC radiated emission limits for Class A digital devices.

Frequency(MHz)	measured at 10 m	
	μV/m	dBμV/m
30-88	90	39
88-216	150	43.5
216-960	210	46.4
>960	300	49.5
>1 Ghz	300(AV)	49.5(AV)
	3000(PK)	69.5(PK)

2.5.2 Requirements for Commercial Products Marketed outside the United States

The International Special Committee on Radio Interference (CISPR) is main agent for governmental EMC requirements outside the United States. CISPR 22, which is the widely used standard, sets limits on radiated and conducted emissions of Information Technology Equipment (ITE). The limits have two classes: Class A and Class B.

The CISPR 22 (EN 55022) conducted emission limits, being the same as FCC conducted emission limits, are given in Tables 2.4 and 2.5. The CISPR 22 (EN 55022) radiated emission limits, on the other hand, are given in Table 2.8 for Class B ITE equipment and in Table 2.9 for Class A ITE equipment.

Table 2.8. CISPR 22 radiated emission limits for Class B ITE equipment (10 m).

Frequency(MHz)	μV/m	dBμV/m
30-230	31.6	30
230-1000	70.8	37

Table 2.9. CISPR 22 radiated emission limits for Class A ITE equipment (10 m).

Frequency(MHz)	μV/m	dBμV/m
30-230	100	40
230-1000	224	47

Chapter 3

EMI Modeling of onboard LRT Equipment

The advent of semiconductor devices made it possible to easily control the desired output parameters in electronic systems, but it brought a new challenge to power electronics. In the design process, more technological parameters such as efficiency and EMC should be considered in addition to external performances. Because a semiconductor inverter is employed on board LRT trams, RF EMFs are expected to appear resulting in some EMI problems. Onboard RF devices emit RF signals either by conduction or radiation. LF EMFs appearing on board LRT trams are other source of EMI that can affect biological functioning of organisms and interfere with other sensitive electronic devices. The overall interference from certain components of the system, however, can not be studied at onece. This is because these components respond differently in LF and HF ranges. Hence separate consideration of these two ranges is necessary.

Modeling of onboard LRT equipment is required before the real EMI analysis. Modeling is the act of representing a real complex system on smaller and simplified scales. Onboard LRT devices can have many different models for EMI analysis. Development of complex models is required to get accurate results that are close to the real system phenomena. Nevertheless, this has some challenges including inaccessibility of all required data and limited memory and solver time of simulating tools. Thus, a compromise must be made between the complexity of the models and the required precision. Before modeling, onboard LRT devices relevant to the study are overviewed.

3.1 Overview of LRT Equipment

There are two kinds of railway electrification systems: DC (direct current) and single phase AC (alternating current). AA LRT adopts DC 750 V electrification. The vehicles are 70% low-floor articulated 6-axle modern trams, consisting of three, bi-directional driving [19].

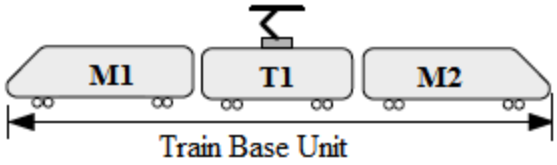

Figure 3.1. Parts of the tram [Author].

The LRT tramcar unit consists of three modules: two M_c modules (motor car with driver's cab) and one central T_p module (trailer without driver's cab and with pantograph). The pantograph installed on top of the trailer module collects current from the catenary of DC 750 V. It is connected to the traction inverter via high speed circuit breaker (HSCB). Each M_c car is equipped with a traction inverter for supplying power to the two traction motors on local bogie i.e one traction inverter drives two motors. With the use of these inverters, DC voltage is converted to three phase AC voltage with Variable Voltage and Variable Frequency (VVVF). Traction motor drives the axles through gear transmission unit. When braking, energy is fed back to power network by the process of regenerative braking; or it is depleted by brake resistor. The general schema of power flow in the vehicle is illustrated in Fig. 3.2.

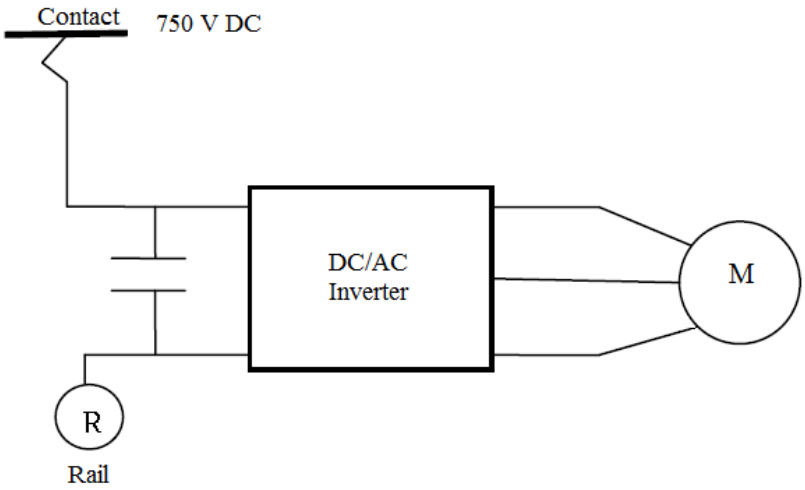

Figure 3.2. Power flow diagram.

Line contactor, Insulated Gate Bipolar Transistor (IGBT) inverter, chopper power unit, logic control unit and filter capacitor are the main constituents of the traction inverter. Its rated power is 2×130kW, and the rated input voltage of main circuit is DC 750 V. Control circuit of the inverter has DC 24 V as rated input voltage. In addition to the traction inverter, an auxiliary

static inverter providing power supply for onboard-tram auxiliary devices also exists. The drive system uses a six pulse inverter with a high switching frequency device, IGBT [19].

The induction motor employed in AA LRT is 3-phase squirrel cage asynchronous traction motor. It has two main electrical components: squirrel-cage rotor and stator. The stator is wound for 6 poles. The windings are geometrically spaced 120° apart. Each motor has rated power of 130 kW, rated voltage of AC 3X500 V, rated current of 210 A, frequency of 71 Hz, and 1800 r/min rated rotation speed [19].

3.2 Analytical Models of EMFs

Generally, analytical methods are used to calculate EMFs generated by simple structures (rectilinear sources). Analytical models lead to a mathematical expression which clearly shows the field's variation with some parameters. Hence it is recommended to apply analytical methods for simple structures, for software tools do not provide the insight that analytical method provides. For very complex systems, however, analytical methods would be tedious or infeasible and hence application of numerical methods by the help of simulating software is mandatory.

This thesis adopts numerical methods. Nonetheless, some analytical formulae for computation of EMFs from simple structures are stated, as well. Those formulae are not directly applied in practical simulations because software tools take over the task. But they are mainly used as theoretical backgrounds. Here, both ELF and RF EMFs are discussed. In ELF range, electric and magnetic fields are treated separately, and the fields may be static or time-varying but still with very low frequency (0-300Hz). In RF range, electric and magnetic fields travel combined to a single field: EM field.

3.2.1 Calculation of Static Electric Fields around a Strait Charged Wire

The existence of electric charge in conductor lines produces electric fields in their vicinity. These charges are due to the voltage difference with respect to ground. For a straight uniformly charged wire, the intensity of electric field at a point of interest *P* can be calculated analytically. In Fig. 3.3 is a straight positively charged wire with a linear charge density of λ c/m. After some integral derivations, the intensity of electric field $\mathbf{E}_p$ is stated as follows.

$$\mathbf{E}_{\text{px}} = \frac{\lambda[\sin\alpha_2 - \sin\alpha_1]}{4\pi\varepsilon h}\mathbf{a}_{\text{x}}$$

$$\mathbf{E}_{\text{py}} = \frac{\lambda[\cos\alpha_1 + \cos\alpha_2]}{4\pi\varepsilon h}\mathbf{a}_{\text{y}}$$

$$E_p = \sqrt{E_{px}^2 + E_{py}^2} \tag{3.1}$$

If the point is along the perpendicular bisector of the wire, $\alpha_1 = \alpha_2$

$$\mathbf{E}_{\text{px}} = 0$$

$$\mathbf{E}_{\text{py}} = \frac{\lambda\cos\alpha_1}{2\pi\varepsilon h}\mathbf{a}_{\text{y}}$$

And if the wire has infinite length, $\alpha_1 \approx \alpha_2 \approx 0$

$$\mathbf{E}_{\text{py}} = \frac{\lambda}{2\pi\varepsilon h}\mathbf{a}_{\text{y}} \tag{3.2}$$

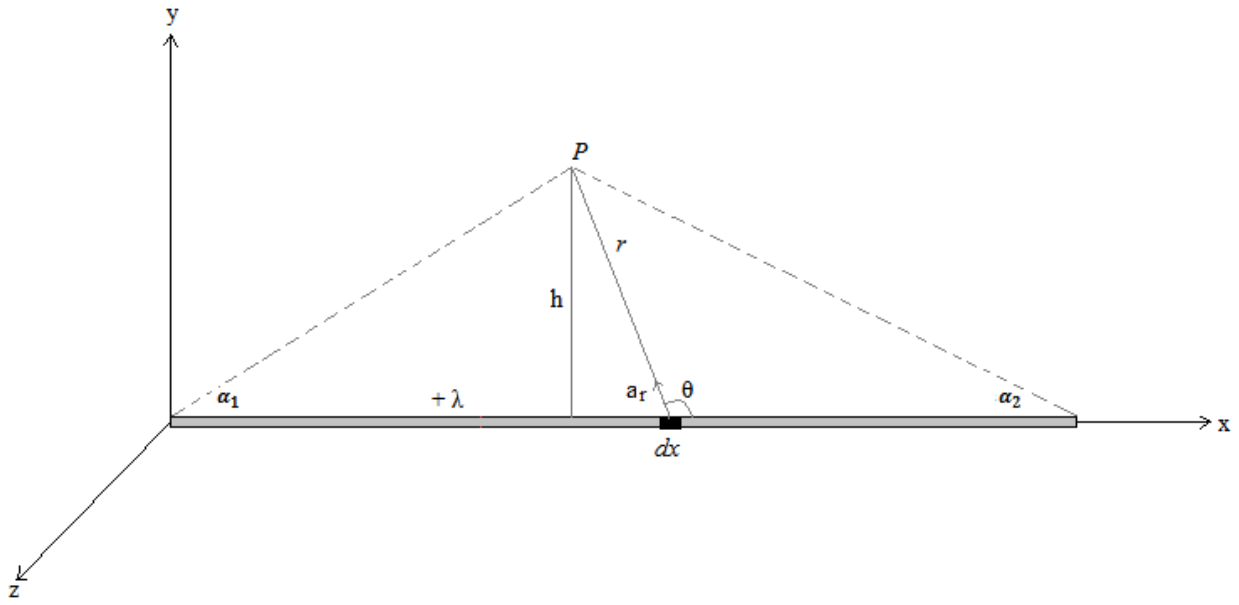

Figure 3.3. A straight uniformly charged wire.

By superposition theorem, for a line with n conductors, the intensity of electric field **E** produced by the line is equal to the sum of the fields separately produced by each conductor. In order for

electric field around a conductor to be estimated, surface charge density of the conductor must be predetermined.

In real systems of LRT, however, it is hard to measure surface charge densities of conductors. Determination of voltage level of the conductors with respect to ground is an easier technique of electric field estimation. When energized, Overhead Contact System (OCS) of LRT establishes potential difference with respect to the ground. The contact lines of AA LRT have DC 750 V. This is the cause of static electric field generation. The tram sweeps across these fields while in motion.

3.2.2 Calculation of ELF Magnetic Fields

Computing ELF magnetic field analytically is based on the calculation of the current that causes it. The magnetic field has the same frequency as that of the current, but its magnitude is independent of frequency because it mainly consists of induction fields. DC currents generate static magnetic fields whereas AC currents result in time-varying magnetic fields. Therefore, it is useful to develop separate analytical models for these kinds of field sources. Review of the fundamental formulae based on which emission models are derived is crucial before that task.

The magnetic field strength generated at a distance *r* by a differential element length *l* with current of *I* can be expressed by the relationship of Biot-Savart Law.

$$\mathbf{dH}_{\mathrm{p}} = \frac{I}{4\pi}\frac{\mathbf{l}\times\ \mathbf{a}_{\mathrm{r}}}{r^2} \tag{3.3}$$

It is interesting to see that Biot-Savart magnetic field is just the same as the $1/r^2$-dependent term in Eq. (2.9c), the induction field. The $1/r$-dependent term (radiation field) is practically less significant at LF and hence it can be ignored.

Static magnetic fields

An example of a structure expected to generate static magnetic field is a straight line of finite length with constant current running through it. The magnetic field strength created by that line having length $\mathscr{L}$ is derived by dividing the line into small differential lengths and integrating all corresponding differential magnetic fields along the line to get the total field as illustrated in the following figure.

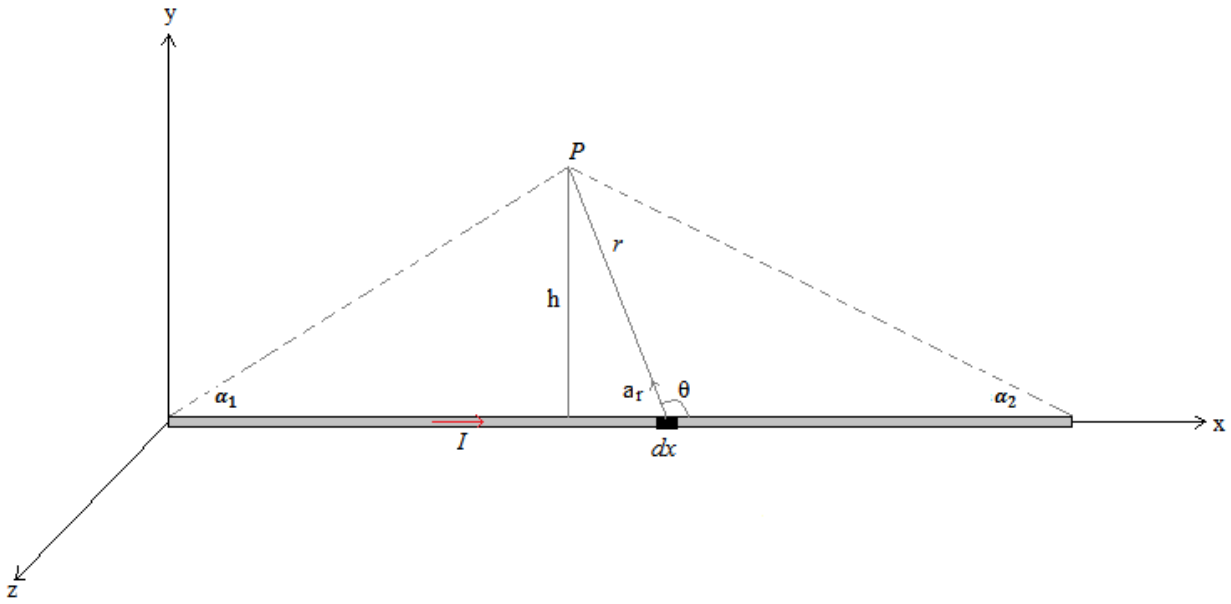

Figure 3.4. A line of finite length, $\mathscr{L}$, with constant current running along it.

The magnetic field strength at point *P* is thus expressed as follows:

$$\mathbf{H}_{\mathrm{p}} = \frac{I}{4\pi h}[\cos\alpha_1 + \cos\alpha_2]\mathbf{a}_{\mathrm{z}} \tag{3.4}$$

where *h* is the perpendicular distance between the line and point *P*. From Eq. (3.4), one can deduce that the total magnetic field generated is directly related to the amount of current but inversely proportional to measuring distance. If the two ends of the line are relatively much longer than the perpendicular distance between the line and the point of interest *P*, the two angles, α_1 and α_2, can be approximated to zero leading to the simplified formula in Eq. (3.5). As we can see from Eq. (3.5), the amount of magnetic field depends only on the current and the perpendicular distance but not on the two line ends.

$$\mathbf{H}_{\mathrm{p}} = \frac{I}{2\pi h}\mathbf{a}_{\mathrm{z}} \tag{3.5}$$

Both static and time varying magnetic fields are governed by the above formulae, the only difference being in their frequency.

Time-varying magnetic fields

Time-varying magnetic fields are caused by a conductor element through which AC current flows. The circuit may be single-phase or three-phase. Time-varying magnetic field strength emitted by electrical circuits is directly proportional to the magnitude of electrical current.

In AA LRT tram, two three-phase circuits extend from the inverter block to each propulsion system. Because of this fact, three phase conductors are considered to analytically estimate the corresponding time-varying magnetic fields. A cross-sectional view of one three-phase cable, together with the corresponding field components, is pictured in Fig. 3.5. Three separate wires of three-phase system are said to make a single circuit. In a three-phase system, each of the three-phase currents generates magnetic field. The phase currents and corresponding field vectors are 120° apart from each other. Single-phase or three-phase circuits generate almost zero net field emission as the balanced currents running along them sum up to zero, hence the corresponding magnetic fields canceling up. The cancellation effect depends on how close the conductors are to each other. If they are not much close to each other, net magnetic field appears as a result of the difference in the perpendicular distance of each wire from the point where magnetic fields are measured.

In spite of the natural cancelation, derivation of expressions for magnetic fields generated by three-phase functional currents is crucial, helping analysis of nearby resultant fields. Let coordinates of conductors *A, B* and *C* in three-phase circuit be x_A, y_A, x_B, y_B, x_C, y_C (Fig. 3.5 shows coordinate systems of only conductor *A*). Let also the coordinates of measuring point *P* be x_P and y_P. The wire radius, r_o, is assumed to be much less than the other transverse linear measurements. The conductors carry symmetric current system i_A, i_B, i_C which is expressed as follows.

$$i_A = I_m \sin \omega t \tag{3.6a}$$

$$i_B = I_m \sin(\omega t - {}^{2\pi}/_{3}) \tag{3.6b}$$

$$i_C = I_m \sin(\omega t + {}^{2\pi}/_{3}) \tag{3.6c}$$

Where,

I_m: maximum current [A]

ω: pulsation [rad/s]

A, B, C –phase conductors of onboard power cables

i_A, i_B, i_C –phase currents

x_P – distance between the y axis and measurement point *P*

x_A – distance between *phase-A* wire and y axis

y_A – distance between *phase-A* wire and x axis

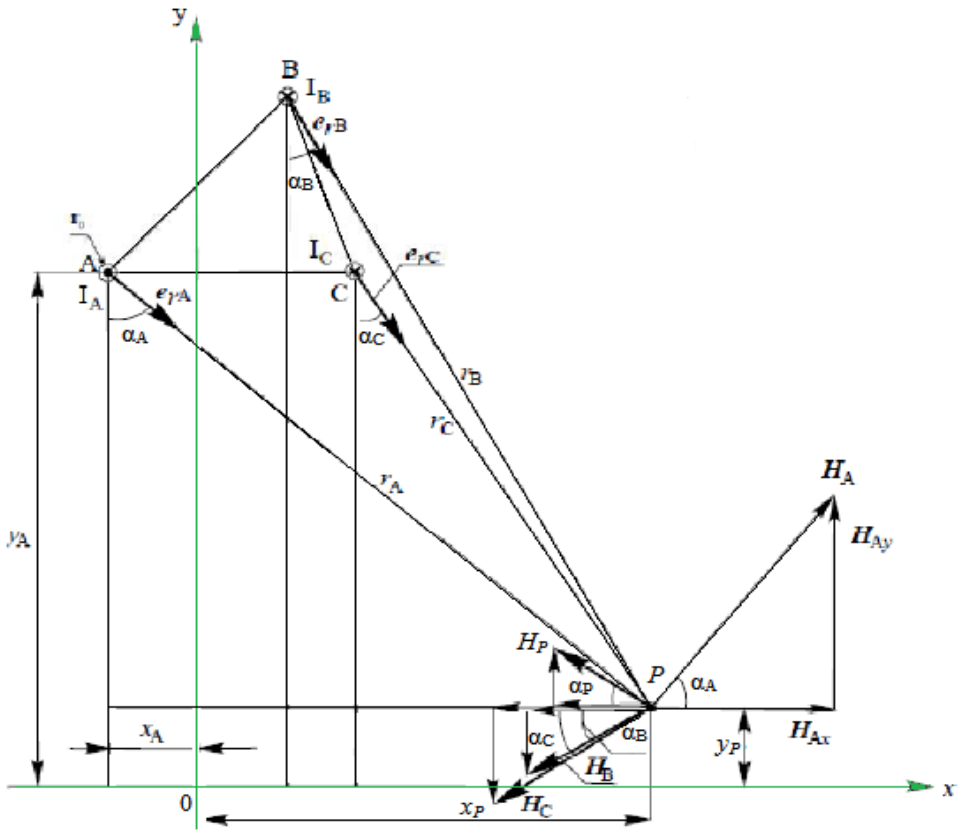

Figure 3.5. Magnetic field emitted by three-phase cable [5].

Suppose that the positive current direction is out of the page and the negative one into the page. The resultant magnetic field is just a vectorial sum of individual fields. At any instance of time, not all currents reach their maximum value as they are 120° out of phase. Since the corresponding field vectors are 120° out of phase too, their vectorial summation is carried out considering those cases (see Eq. 3.7).

$$\mathbf{H_P} = \mathbf{H_A} + \mathbf{H_B} + \mathbf{H_C} \tag{3.7}$$

The magnetic field of a straight endless wire with running current I at a distance r is already stated in Eq. (3.5) (h is replaced with r here, and the unit vector **a** with **e**). The resultant magnetic field is a vectorial sum of the three individual fields.

$$\mathbf{H}_\mathrm{P} = \frac{1}{2\pi}\left(\frac{I_A}{r_A}\mathbf{e}_\mathrm{rA} + \frac{I_B}{r_A}\mathbf{e}_\mathrm{rB} + \frac{I_C}{r_A}\mathbf{e}_\mathrm{rC}\right) \tag{3.8}$$

Where,

r_A, r_B, r_C – distances of point P to conductors A, B and C

$\mathbf{e}_\mathrm{rA}$, $\mathbf{e}_\mathrm{rB}$, $\mathbf{e}_\mathrm{rC}$ – unit vectors corresponding to these distances.

The distances expressed in terms of their coordinates are put as follows:

$$r_i = \sqrt{(x_P - x_i)^2 + (y_P - y_i)^2}$$

Where,

r_i – wire distance from the point;

x_i, y_i – coordinates of this wire center;

i - indices of phases line;

Angle α (shown in Fig. 3.5) is found as follows:

$$\alpha_i = \arctan\frac{x_P - x_i}{y_P - y_i}$$

Projections of the magnetic field strength vector onto the coordinates, H_x and H_y, are obtained as follows:

$$H_x = H_{Ax} + H_{Bx} + H_{Cx}$$
$$H_y = H_{Ay} + H_{By} + H_{Cy}$$

The following equations are used to calculate the module of vector **H** and the angle α_p (with the x axis):

$$H_P = \sqrt{\left(H_x^2 + H_y^2\right)} \tag{3.9}$$

$$\alpha_P = \frac{H_y}{H_x} \tag{3.10}$$

Magnetic flow density B is related to H as $B = \mu H$, where μ – magnetic permittivity of the medium (for vacuum, $\mu 0 = 4\pi \times 10^{-7}$ H/m).

3.2.3 Calculation of RF EM Emission from Simple Structures

For electrically short wires, simple emission models are developed considering CM and DM currents. A pair of parallel wires of length $\mathscr{L}$ and separation s is considered as shown in Fig. 3.6. The wires lie on xz plane and are parallel to z axis. Since frequency domain emission model is considered, the currents ($\hat{I}_1$ and $\hat{I}_2$) are put in phasor form [1]. The currents are decomposed into DM and CM components as in the following equations.

$$\hat{I}_1 = \hat{I}_C + \hat{I}_D \tag{3.11a}$$

$$\hat{I}_2 = \hat{I}_C - \hat{I}_D \tag{3.11b}$$

Rearranging Eq. (3.11), the following expressions are obtained.

$$\hat{I}_D = \frac{\hat{I}_1 - \hat{I}_2}{2} \tag{3.12a}$$

$$\hat{I}_C = \frac{\hat{I}_1 + \hat{I}_2}{2} \tag{3.12b}$$

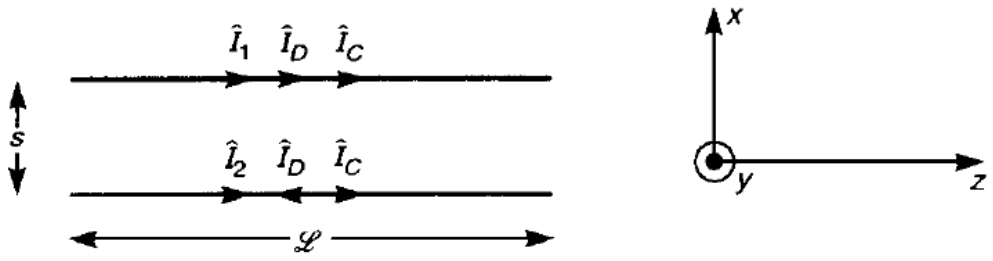

Figure 3.6. Parallel conductors [1].

For current segments that are very short electrically, the two wires are assumed to be just two parallel Hertzian dipoles. Radiated electric field of each wire is maximum broadside to the antenna (θ=90). The total radiated electric field in the plane of the wires and broadside to the cable (worst case) is obtained by adding radiated fields of the individual wires for both CM and DM currents [1]. A measurement point in the plane of the conductors is defined. It is in the far field of each antenna and at a distance *d* from a point that is midway between the conductors.

Now radiated emissions due to DM and CM currents are separately stated. DM currents flow in opposite direction and hence the net electric field radiation is the difference of the individual fields. As long as the wires are not collected, a net electric field will result. Detailed derivation of electric field radiation from DM currents is conducted in [1], and the final result in its simplified form is stated as follows:

$$\hat{E}_{D,max} = j2\pi \times 10^{-7} \frac{f\hat{I}_D L}{d} e^{-j\beta_0 d}\left\{e^{j\beta_0 s/2} - e^{-j\beta_0 s/2}\right\}$$

$$= -4\pi x 10^{-7} \frac{f\hat{I}_D L}{d} e^{-j\beta_0 d} \sin\left(\frac{1}{2}\beta_0 s\right)$$

Assuming, $\sin(\frac{1}{2}\beta_0 s) \cong \frac{1}{2}\beta_0 s$,

$$\left|\hat{E}_{D,max}\right| = 1.316 \times 10^{-14} \frac{\left|\hat{I}_D\right| f^2 L s}{d}$$

For the loop area $A = \mathscr{L} s$,

$$\left|\hat{E}_{D,max}\right| = 1.316 \times 10^{-14} \frac{\left|\hat{I}_D\right| f^2 A}{d} \quad (3.13)$$

The CM current radiation is obtained by noting that CM currents flow in the same direction and the radiation of each Hertzian dipole adds up to total electric field.

$$\hat{E}_{C,max} = j2\pi \times 10^{-7} \frac{f\hat{I}_C L}{d} e^{-j\beta_0 d}\left\{e^{j\beta_0 s/2} + e^{-j\beta_0 s/2}\right\}$$

$$= j4\pi x 10^{-7} \frac{f\hat{I}_C L}{d} e^{-j\beta_0 d} \cos(\frac{1}{2}\beta_0 s)$$

Assuming that the wire spacing s is electrically small, so that $\cos(\frac{1}{2}\beta_0 s) \cong 1$,

$$\left|\hat{E}_{C,max}\right| = 1.257 \times 10^{-6} \frac{\left|\hat{I}_C\right| f L}{d} \quad (3.14)$$

3.3 Software Modeling

In this thesis, numerical methods are adopted by the help of software tools since the system under consideration has some complexities. Thus, all main works of this thesis are delegated to software simulations. Numerical computations are carried out based on a generic algorithm illustrated in the following picture.

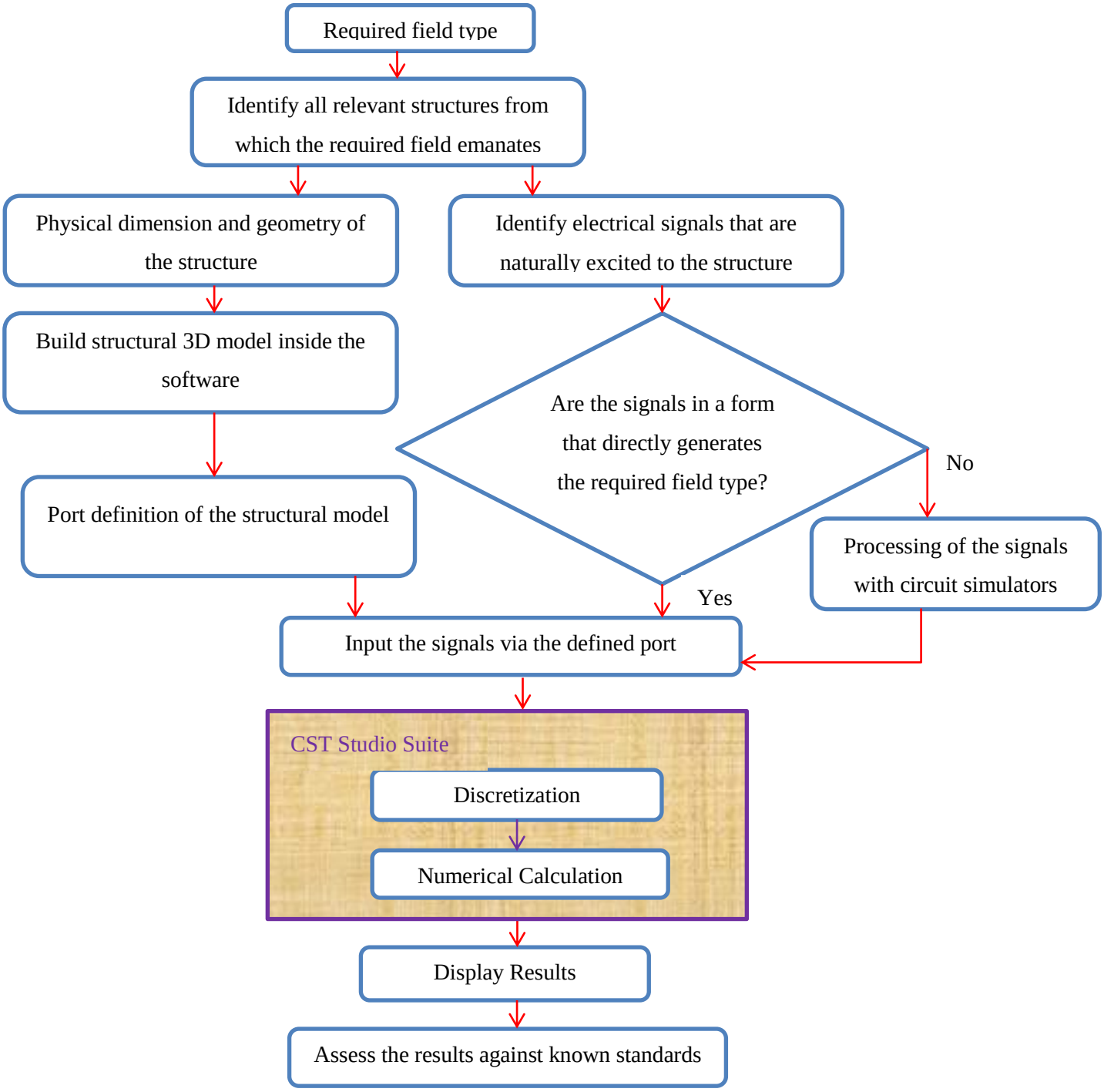

Figure 3.7. Flowchart for software modeling.

The amount of EM radiation from a given structure depends on geometry of the given structure and magnitude of electrical signals excited to it. Hence both physical and electrical parameters of a given system should be determined in order to estimate EM emission from that system. After physical parameters (dimensions, geometry and positioning) of a given structure are identified, a

3D model is built inside the software, and ports are defined on the model in order to excite it with predefined electrical signals. Some electrical signals need preprocessing before they are directly applied to developed 3D models. This is because the required signals generating the relevant field types may not be directly stated in the given specifications. Hence they must be derived from other explicitly-stated irrelevant signals. Another reason is that only some portion of the signal may be more relevant to a specific study area, with the rest ones being irrelevant or ignorable. Because of these facts, some electrical data should be preprocessed in such a way that all relevant signals are extracted with the help of circuit simulators. If signals which are responsible for generation the contemporary fields are explicitly stated, however, further processing is not required.

With 3D geometrical models built and some electrical data preprocessed and fed to the model via defined ports, the software is made to run, and EMFs around the structure are computed numerically. The software (CST Studio Suite) goes its own simulation steps to carry out a specific task. As is observed in Fig. 3.7, *discretization* and *numerical calculation* are the steps followed inside CST Studio Suite to conduct simulation.

As discussed previously, there are many kinds of EMFs emanating from electrically excited structure. Some cables of the tram predominantly generate one kind of field whereas others generate different kind, depending on their excitation signal. As the corresponding EMI impact also varies depending on the field type, those kinds of fields should be studied separately. In developing 3D model and identifying input data, all assumed physical and electrical parameters are those that are capable of generating the field type under consideration. All irrelevant structures are excluded, hence an ease in computing the required field. Separate consideration of those field kinds not only brings an ease in classification of EMI impacts but also saves memory by enabling one to consider only relevant parameters. Here in this thesis, there are three kinds of EMFs to be considered separately.

1. Static magnetic field
2. Static electric field
3. RF EM fields

Both static magnetic and static electric fields are under the category of ELF EMFs whereas RF EMFs result from HF signals. Although small in magnitude, ELF time-varying magnetic fields

are generated from three-phase power cables too. It is the functional three-phase AC currents that lead to generation of ELF time-varying magnetic fields. Their contribution to the whole system is insignificant, however. Their field strength dramatically decays in centimeters rang because the three-phase currents (being 120° out of phase) induce corresponding magnetic fields which are 120° out of phase too. Hence the vectorial sum of the fields is almost zero due to cancellation effect. Some field exists only when the conductors are placed some distance apart. This field strength is still generally low compared with other field kinds. Three-phase conductors on board AA LRT trams are much close to each other, their mutual distance not exceeding 1.5 cm. Hence ELF time-varying magnetic fields emanating from them are assumed to be ignorable, and this work focuses on other potentially strong field kinds which are listed above.

3.3.1 Modeling of Static Magnetic Fields

In addition to RF EM spectrum coming out from onboard devices, ELF EMFs are also generated and bring considerable impact on human health and other susceptible systems. Static magnetic fields, static electric fields and ELF time varying magnetic fields are under the category of ELF EMFs. In this subsection, modeling of static magnetic fields on board AA LRT trams is conducted.

Computation of static magnetic fields is helpful to quantify the emission level and predict the potential hazards of the fields. Practically, the interaction of the tram with the overhead contact lines and the far substations results in overall magnetic field pollution. EM emission from contact lines of LRT is already studied by [20] and hence this work focuses on EMIs caused by internal structures of the tram. In the work of [20], the tram was considered as a single straight element, emphasizing on EM emissions from the whole system. But this work focuses on EM distributions inside the tram by dealing with more complex positioning of onboard wires. Independent consideration of the tram as source of EMI is justifiable since it makes partially self-contained system, not permanently fixed to the contact systems.

Prior to structural modeling, a review of vehicle dimensions and wiring arrangement is necessary. Such task helps in identifying the generic structure from which all the three field types (static electric field, static magnetic field and RF EM fields) emerge. But this section specializes into structures giving rise to generation of static magnetic field after reviewing the generic

system. The wire geometry and positioning are derived from already available data specifications and commonsense estimations. Here below is a list of dimensions of the vehicle taken from [19].

- Length of car body ≤30000 mm
- Height of vehicle roof from top of rail (excluding pantograph) ≤3700 mm
- Maximum width of car body 2650 mm
- Height of vehicle floor from top of rail (low floor area, new wheels and empty load) ≤380 mm
- Height of vehicle floor from top of rail (exit and entry areas, new wheels and empty load) ≤350
- Height of vehicle floor from top of rail (raised floor area, new wheels and empty load) ≤900 mm
- Wheelbase (power bogie) 1900 mm
- Wheelbase (unpowered bogie) 1800 mm
- Clear height of passenger compartment ≥1980 mm
- Wheel diameter (new wheel) ≤660 mm
- Wheel diameter (Max. wear) ≤600 mm
- Side doors of passenger compartment 4 pairs per side
- Clear opening of passenger compartment door (width x height) ≥1300×1860 mm

Height of contact line for ground sections from top of rail is generally 4500 mm to 5400 mm. The pantograph's working height varies from 380 mm–2400 mm [19]. In this thesis the pantograph is assumed to have 1000 mm height and the contact lines 4700 mm height. Height of vehicle floor from top of rail varies from 350 mm to 900 mm. But most of the floor portion is assumed to lay on a height of 360 mm to make it uniform. Also, the power cables, which are placed just below the floor, are thought to be 350 mm high from top of the rail.

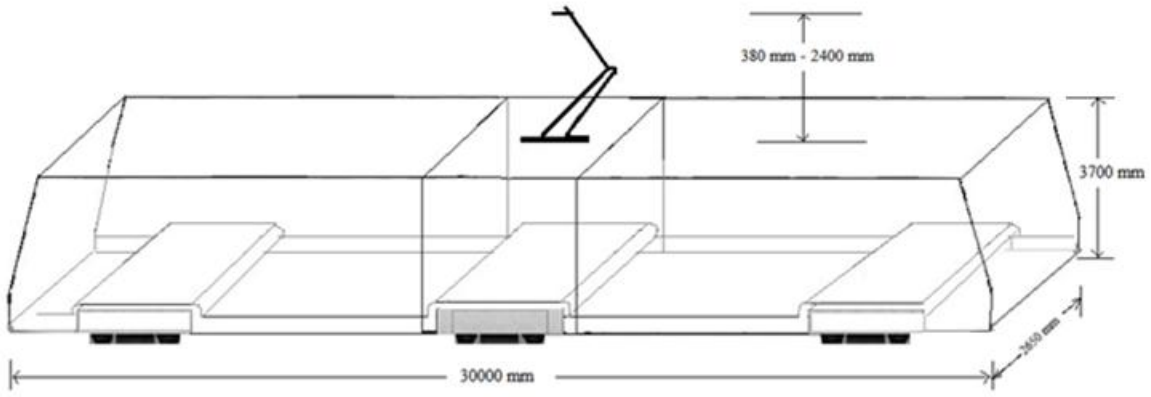

Figure 3.8. Main dimensions of the tramcar [19].

In order to have more exact prediction on the field distributions of the existing system, the dimensions and orientations of the cables should be taken as exact as those installed aboard the trams. The author, however, had very difficult time accessing such information and was compelled to take some approximations as well. Further dimension estimations are made based on the drawing in Fig. 3.8. Three-phase cables interconnect the traction inverter and the motors through the cab cable. Each inverter feeds its respective AC motors that are in the bottom floor of the M_c modules. Two three-phase cables, which go down through the tram body (cab cables), are required for each M_c module as it comprises of two AC motors. Each inverter, hence, branches off into two electrical circuits. The field types generated by three phase cables are LF time-varying magnetic fields and RF EMFs but not static magnetic fields. Hence three-phase power cables are mainly discussed in modeling of RF EMFs. The inverter is almost positioned above the motors, which are located 10 m away from T_p car floor center. Therefore, it is expected to be 10 m apart from the base of the pantograph. The DC-current-carrying wire between pantograph base and traction motor has 90 mm^2 as cross-sectional area. Each side of the path covers a total length of 20 m together with grounding cable. The pantograph is assumed to be 45°-bent and have 1 m height.

The DC current inside the tram body flows from the pantograph base to the inverter and returns back through the ground. One of the rails is used as a ground for the returning current to pass through. Hence grounding conductor is put between the traction inverter and the bottom rail. This grounding conductor passes through the cab cables along the tram body. Knowledge of current magnitude and the path it follows, regardless of electrical devices in between, is

sufficient for prediction of induced magnetic fields. Thus, the DC current can be viewed as if it simply flows from the pantograph to the ground through the specified path. As the required field in this section is static magnetic field, the conductors and wires to be considered here are those that carry DC currents.

The pantograph collects current from the catenary of DC 750 V. It carries rated working current of 1050 A. More than half of the current runs along a DC power cables connecting traction inverters with the pantograph base whilst the rest one feeds auxiliary power supplies for on-board electrical devices (lamps, microcomputers, etc.). Since symmetrically positioned two inverters exist on each tram, the amount of DC current coming from the pantograph and feeding the inverters splits in to two making two parallel paths. The amount of current branching off toward extra path, auxiliary inverter, also splits symmetrically into two in both sides. Both the traction system and auxiliary power supply system contribute to generation of static EMFs. Therefore, the model should include current paths of both main traction system and auxiliary power supply system on two symmetric sides of the tram. The geometrical model in Fig. 3.9 illustrates both current paths: auxiliary power system and traction system current paths. The DC current drawn by the inverters can be derived from available specifications.

$$I = \frac{P_{inverter}}{V_{inverter}}$$

$$= \frac{2 \times 130\ kW}{750\ V} = 346.6\ A \tag{3.15}$$

A current of I = 347 A flows through the traction inverter to each sides of the M_c car. It is known that half of the total current that comes from the pantograph, ½(1050) = 525 A flows to each side of the tram. Out of the 525 A, 347 A was contributed by traction inverter. Hence the remaining 178 A is drawn by auxiliary static inverter on each side. For the sake of simplicity in the final simulation, the current paths which run close to each other (traction system current and auxiliary power supply current) can be modeled as just one path ignoring their distributed nature(See Fig. 4.2). Therefore, the total current of 1050 A entering the locomotive can be seen as if it splits symmetrically to the two M_c cars and sums up at the ground. Among the total 1050 A current, 694 A is contributed by the traction system whereas the rest one is drawn by auxiliary power supply system.

In spite of the variety of EMF sources, the total electric or magnetic fields permeating the surrounding area determines how strong the electromagnetic pollution is. International standards set limits on EM radiations by putting restrictions on the total field strength generated by a given system. Owing to these facts, some coordinate system should be adopted in order to predict the total magnetic fields inside and outside the tram. Figure 3.9 shows the positioning of cables aboard the LRT tram. This 3D geometrical model is generic as it includes geometry of conductors responsible for creation of both static and time varying EMFs. RF problems also share the same geometry but consider only the inverter-motor segment which is expected to carry HF spectrum. This subsection deals with EM problems related to static magnetic fields. Hence only DC current paths and grounding conductors are considered for the time being. Simplification of the structural model in Fig. 3.9 into a one consisting only of elements relevant to static magnetic field is necessary. The model in Fig. 4.2 fulfills this task. It is derived from the 3D structure in Fig. 3.9 by excluding conductors which have no direct relevance to static magnetic fields and collecting parallel DC current paths to a single one. The dimensions of the cables are taken as given above and their geometry as portrayed there. In the final simulation conducted in Section 4.2.1, current paths (current source) are defined on previously developed structures for the purpose of excitation. Current path of each side is excited with a current of 525 A, which is half of the current coming from the pantograph (Fig. 4.2). Finally, the model is run inside the software and the resulting magnetic field around the space is portrayed as a function of coordinate system variables.

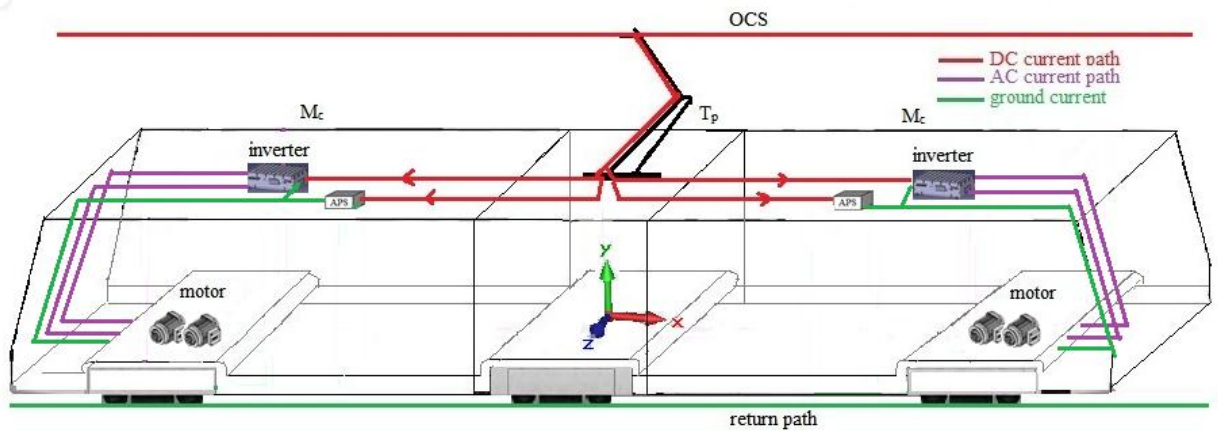

Figure 3.9. 3D view of the LRT tram [Author].

Inclusion of remote substations and contact lines to modeling would make the results more accurate and reliable. However the feeding substations are located at kilometers away from the running tram and this makes the simulation costlier. Thus, the better option to make a compromise is to consider only some portion of the system. The subsystem to be considered includes the LRT tram and little more extending contact systems which are nearer to the running tram. As portions of contact lines get remoter with respect to the running tram, their impact becomes less. Whether they are included or not doesn't bring a great difference to the expected result. Hence assuming the tram is far away from substation, remote substation and contact lines are excluded from simulation. Current sources are defined aboard the tram itself to replace those ones coming from remote substation in the real system.

Inside the EM simulator, electric boundaries are defined in the region beyond which the proposed model can't extend. Fig. 3.10b illustrates how the boundary is configured. The usage of electric boundary helps to make closed circuits in the case of magnetic field simulation. The current paths defined aboard the tram are the only sources of the closed circuit. The height of contact system is considered to be 4700 mm. Since current is assumed to come from one side substation, only the left side of OCS is included in the closed circuit (Fig. 3.10b). The length of that OCS must also be truncated to finite length in final simulation. It has 20 m length in the left direction from the center of the tram. Out of this, the 7 m long extra distance extends beyond the edge of the tram. The model in Fig. 4.2, which was simplified for the purpose of magnetic field simulation, takes into account these assumptions. A little bit extending contact lines and electric boundaries are included in that corresponding software model.

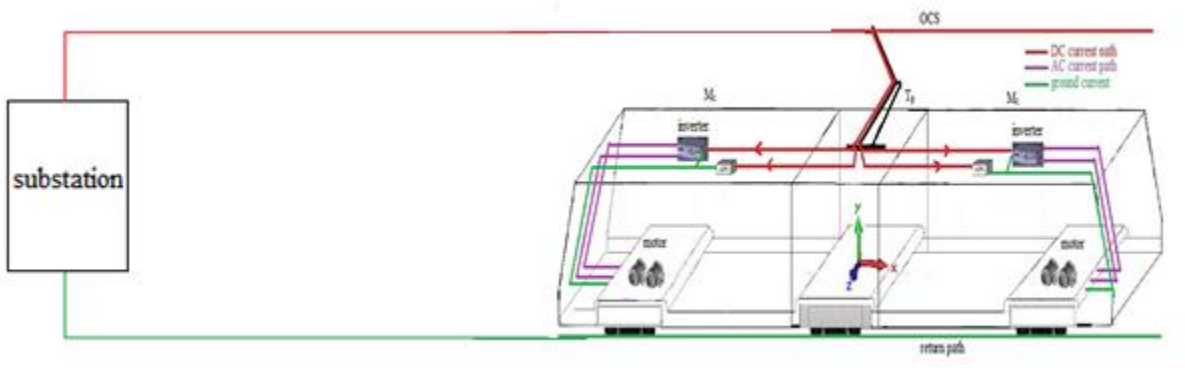

(a)

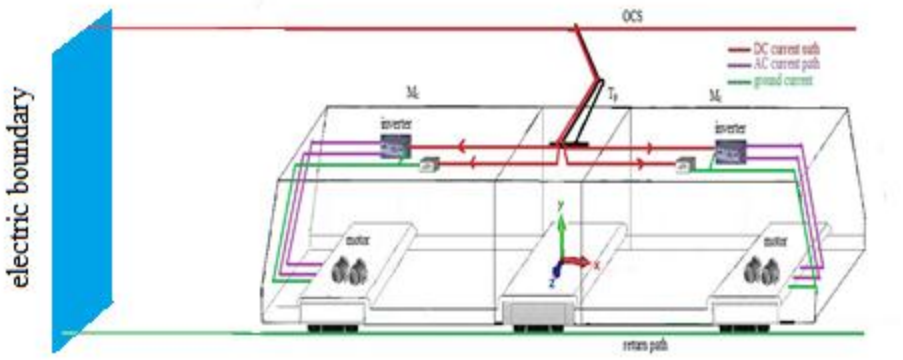

(b)

Figure 3.10. Running tramcar with contact lines. (a) Original full system. (b) Simplified proposed model.

Cartesian coordinate system was employed, for it is a global coordinate system in CST Studio Suite. The origin of Cartesian coordinate system is set at the bottom center of the T_p car as illustrated in Fig. 3.9. It is 360 mm high from top of the rail. The y axis points upward through the T_p module center. x and z axes make a plane parallel to the floor of the tram. The x axis is along the length of the tram. This configuration, being a global coordinate system, is also used for simulation of fields other than static magnetic field: static electric field and RF EMF.

3.3.2 Modeling of Static Electric Fields

Electric field distributions can be estimated from knowledge of voltage difference between two points. There is a voltage difference of 750 V between the catenary and the ground rail. This is expected to generate static electric fields oozing around the contact lines. The fields are always there whether the tram passes through or not. It is required to know how much strong electric field permeates inside the tram when it is connected to the contact system. The model, however, assumes only the contact systems as source of electric field. This is because noticeable voltage difference, which in turn leads to field accumulation, is observed across the contact lines.

For electric field simulation, an equivalent circuit of the structure shown in Fig. 3.11 is developed inside the software and is excited with voltage difference of 750 V. The height of the OCS is taken as 4.7 m on average. The OCS indeed extends far covering a distance of kilometers. However, field strengths due to contact lines at remote area are ignorable compared with those resulting from nearer contact lines. It is also true that the software needs limited space for simulation. Because of those facts, OCS segment of 40 m length was considered. Hence to

estimate electric field strength at a given point on the track, a contact line extending 20 m on both sides (total of 40 m length) was considered. Also, it was assumed as if it were a single track contact line. Actually, the second line of double track has its own contamination to the expected result. Here its impact is excluded.

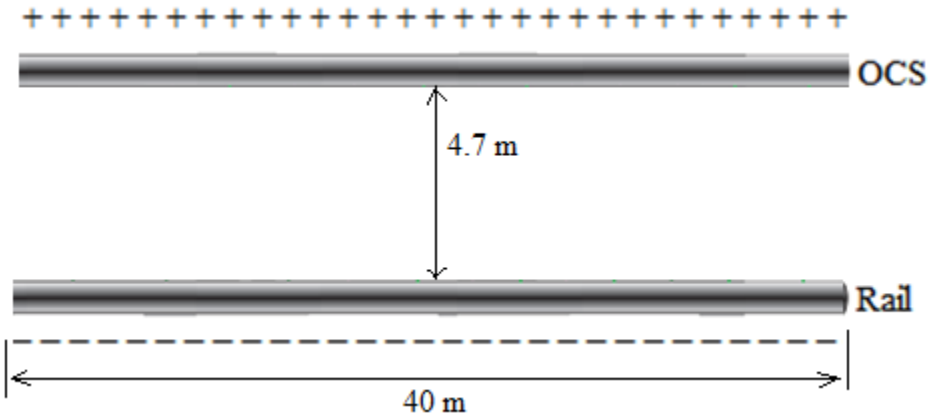

Figure 3.11. Schematic model for electric field simulation.

Cartesian coordinate system was used to measure how the field varies along a given direction. Although not included in the simulation, the tram is assumed to be ideally present, and it is at the bottom center of the T_p car that the origin of the coordinate system is set. The calculation domain of the software extends 20 m far in the positive and negative x axis. The x axis is parallel to the track whereas y axis points upward, and z axis toward the observer (Fig. 4.8).

3.3.3 Modeling of RF EMFs

Up to this point, static EMF problems on board LRT trams have been discussed. The functional frequency of the traction motors is 71 Hz which lies within a range of LF problems. However, EMFs in the range of radio frequencies may also result from intentionally transmitted radio signals and high switching semiconductor devices. High spectral signals generated from the inverters travel along the three-phase power cables coupling to the traction AC motor. The fact that PWM of a semiconductor inverter switches at HF causes a number of problems some of which are the following:

- reflection of voltage waves at the motor terminal, thereby leading to transient overvoltage
- conductivity disturbance in power network

- HF electromagnetic radiations which may couple to sensitive electronic devices mounted aboard the LRT tram

Stray capacitances in the motor drive system have negligible size at LF but considerable impact at HF. They act as low impedance paths for circulating HF CM current. CM current is the cause of conducted and radiated interference in the power circuit. Radiated interferences are mainly discussed in this section with special focus on three-phase power lines between inverter and motor. Figure 3.12 portrays an inverter-fed induction motor with EM noise radiating from interconnecting cables.

Practically, most of products contain additional circuits in order to suppress HF components. It was not possible to access internal structure of the LRT tram and hence all preventive mechanisms including power filters were assumed to be absent. By such assumption, this thesis considers the worst-case scenario and analyzes inherent noises of the system observed when no further techniques of EMI reduction are employed. Furthermore, the impact of metallic enclosures on radiating EM energy is neglected. The core assumptions made in this section are generalized as follows.

- No filter was employed between the traction inverter and motor.
- The impact of metallic shields enclosing the cables was too small.
- The entire CM current makes a path through the three-phase cable between inverter and motor.
- No external systems capable of emitting RF energy (Radio Communication Systems) were included; only the cables installed aboard the tram were considered.

Bearing in mind these assumptions, this thesis takes the inverter-motor system as the main target.

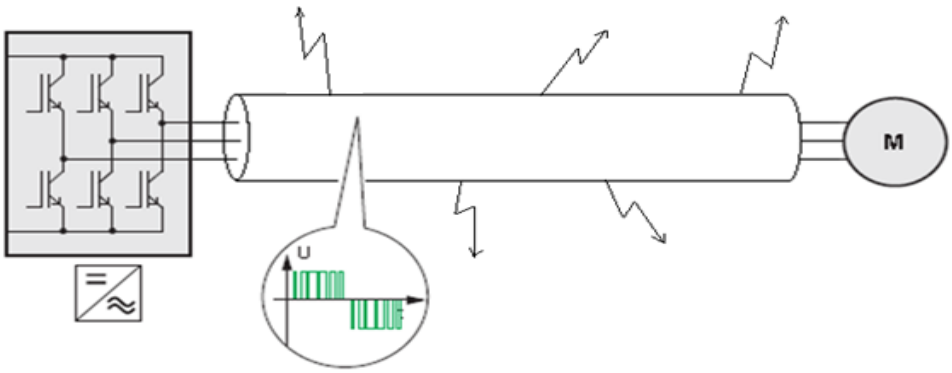

Figure 3.12. PWM inverter-fed induction motor with long cables emitting RF energy.

Prior to 3D model design, identification of geometrical positioning of the structure expected to give out RF emission and preprocessing of the electrical signal excited to that system should be conducted first.

Geometrical positioning of the three-phase cables

The model in Fig. 3.9 is just generic and can also be applied for RF problem analysis. In the case of RF emission, however, only the components responsible for RF emissions (three-phase power cables) are considered. An overview of positioning of the three-phase cables relative to other onboard devices was made in Section 3.3.1. There are two three phase circuits on each side of the tram. The total length of one three phase cable is almost 10 m. Each of the three conductors in a single three-phase cable has 70 mm^2 as cross-sectional area. Their mutual distance is assumed to be 1.5 cm. The dimensions and geometry employed in the software model are the same as those ones depicted in the following figure.

Figure 3.13. Three-phase cable geometry.

One point to be noted here is that the currents that cause RF emissions are not the functional DM currents which are explicitly stated in data specifications. HF CM current resulting from PWM inverter is the main cause of RF emissions. Hence such CM current must be extracted from LF functional currents prior to the next RF analysis. Processing of LF functional currents is required in order to extract RF signals that are probably present in the system. Finally, they are used as direct input for the 3D model developed inside the software.

Preprocessing of electrical signals

The LRT tramcar induction motor has a rating of 130 kW, 500 V and 71 Hz. It is fed by PWM inverter with output power of 2x130 kW. The voltages and currents outputted by the inverter travel along the interconnecting power cable and appear at the motor terminal. The output

voltage of the inverter is not pure sinusoidal but has HF harmonics due to the PWM effect. The fundamental component of the output voltage is equal to voltage rating of the motor.

The drive system uses a six-pulse inverter with IGBT. Three sinusoidal control voltages (reference wave V_r, frequency f_r) that are 120° out of phase are compared with a saw tooth voltage waveform (carrier wave V_c, frequency of 4 kHz) to produce the gate signals of the inverter [21]. The switching instants of the modulated pulse correspond to the inter section of V_c and V_r waves. A comparator is employed to mix the carrier and reference waves. The comparator output is high whenever the sinusoidal wave is greater than the saw tooth wave, otherwise it is low. The ratio of V_r/V_c is called the modulation index (MI). The fundamental component of the output voltage is directly related to MI. Thus it is possible to vary the output voltage by varying MI. The output voltage and the reference sinusoidal voltage have the same frequency.

The inverter outputs fundamental component of line voltages with rms value of 500 V which is equal to the motor input.

$$V_{ab1(rms)} = V_{bc1(rms)} = V_{ca1(rms)} = 500\ V \tag{3.16}$$

Line-to-line pick voltages of the fundamental component are stated as follows:

$$V_{ab1(peak)} = V_{bc1(peak)} = V_{ca1(peak)} = 500\sqrt{2}\ V$$

$$= 707\ V \tag{3.17}$$

The fundamental component of the phase voltages are reduced by $\sqrt{3}$ factor from the line voltages and lag by 30 degree.

$$V_{a1(peak)} = V_{b1(peak)} = V_{c1(peak)} = \frac{707}{\sqrt{3}}\ V = 408\ V \tag{3.18}$$

The phase voltages are related to MI as follows:

$$V_{a(peak)} = MI\,\frac{V_{dc}}{2} \tag{3.19}$$

Where V_{dc} is equal to 750 V. Thus, MI is obtained by rearranging this equation:

$$MI = \frac{V_{a(peak)} \times 2}{V_{dc}} = \frac{408 \times 2}{750}$$

$$= 1.09 \simeq 1$$

The following figures illustrate phase voltages at the inverter output. They were found from equivalent circuit of an inverter in LT spice software by setting all the parameters to the given values: f_r=71 Hz, carrier frequency=4 kHz, $V_c = V_r = 2.5$ V.

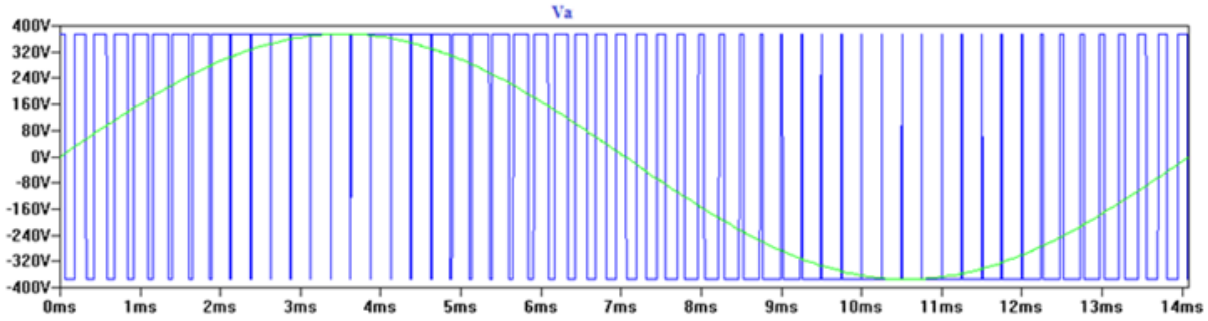

(a)

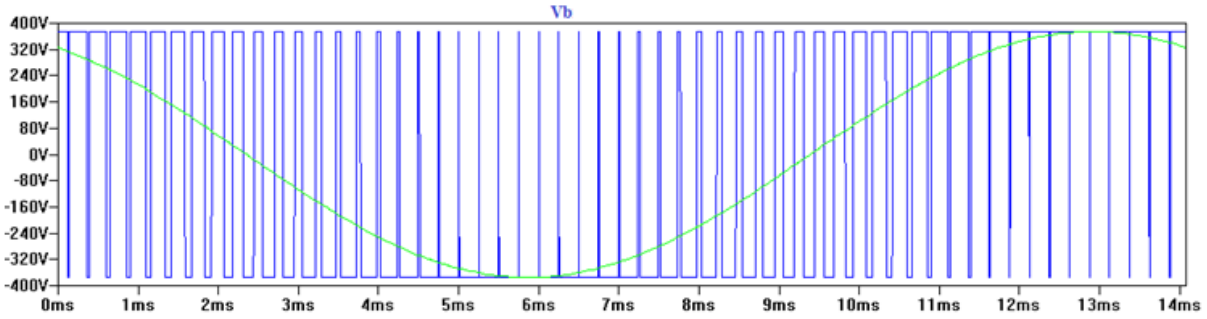

(b)

Figure 3.14. Inverter-output phase voltages with fundamental components: (a) V_a. (b) V_b.

In Fig. 3.14 are two of the phase voltages appearing at the inverter terminal (V_a and V_b) with their fundamental component. The third phase voltage, V_c, is identical in form to those voltages, its only difference being 120° phase difference. The phase voltages are not pure sinusoidal as indicated. High spectral components are present due to the steep rising edges of the voltage output. These are the causes of overvoltage and EMI.

The line voltage is just the difference between the phase voltages. One of the line voltages, V_{ab}, for example is obtained by subtracting V_b from V_a. In the following figure, one line voltage resulting from the difference between the voltage waveforms shown in Figures 3.14a and 3.14b is depicted. The other two line voltages are obtained the same way from their respective phase

voltages. As the phase voltages are 120° apart to each other, so are the corresponding line voltages.

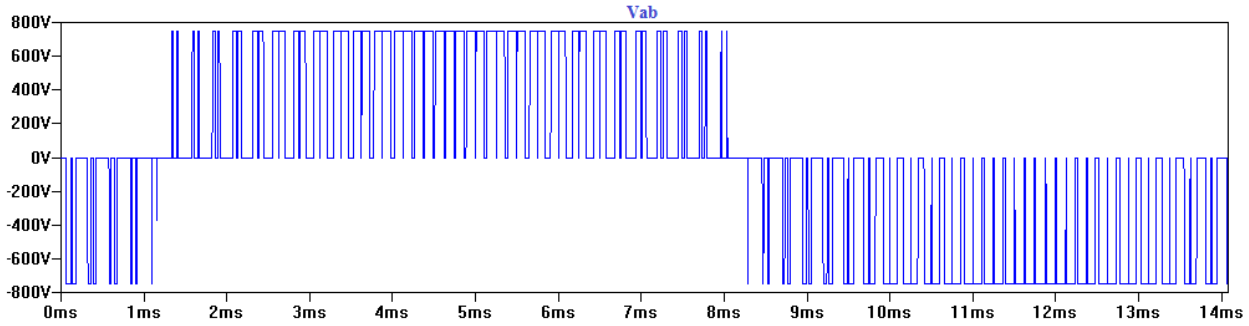

Figure 3.15. One of the line voltage waveforms, V_{ab}.

Now, let's also see what the line currents look like. Knowledge of motor winding impedance is required in order to determine line currents. Detailed derivation of the winding impedance from available data is stated in Appendix A. As calculated in Eqs. (A.4) and (A.6), each motor winding has a resistance of R = 1.56 Ω and inductance of L = 1.69 mH. Having this information in mind, it is possible to model a three-phase circuit which uses the above phase voltages as input. Figure 3.16 represents the three phase equivalent circuit. The CM current leaks out from the star point of the motor and returns back through metallic enclosures, ground conductors and the like.

Three-phase line currents at PWM inverter output, differently from purely sinusoidal currents, are not balanced. CM current inherently results from PWM inverter-fed machines. At the star point of the machine, instantaneous summation of all the line currents is non-zero. Hence an impedance, which characterizes the CM current path, would be established between the star point and ground. This impedance is due to inherent stray capacitance between the star point and ground wire (or stator frame). Such stray capacitance was not easily accessible because it was not possible to conduct a direct test on the LRT tramcar induction motors. Hence the only option considered was to use rough approximations to fill this data gap. Based on different motor specifications with similar capacity, stray capacitance of AA LRT tramcar induction motor was approximated to 12 nF. After setting it to 12 nF, the circuit in Fig. 3.16 was simulated, and the resultant line currents were obtained.

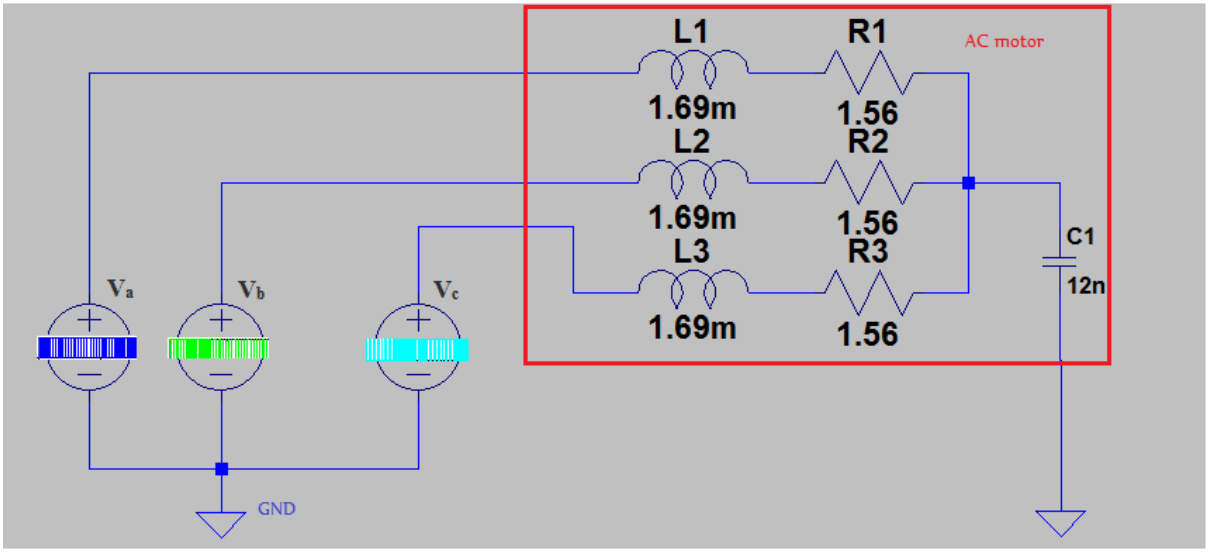

Figure 3.16. Three-phase equivalent circuit.

To a large extent, the motor appears as an inductor to the output voltages of the inverter. As an inductor has higher impedances at high frequencies, most of the current drawn by the motor is due to LF components in the PWM inverter output. This is why the line currents, which are obtained by simulating the circuit in Fig. 3.16, somehow resemble sinusoidal waves (Fig. 3.17). These currents circulate around the three-phase lines. If the line currents were pure sinusoidal, they would be balanced, and there would be no CM current leaking out from the star point. Because of the PWM nature, however, they have small iregularities which in turn lead to generation of CM current (Fig. 3.17).

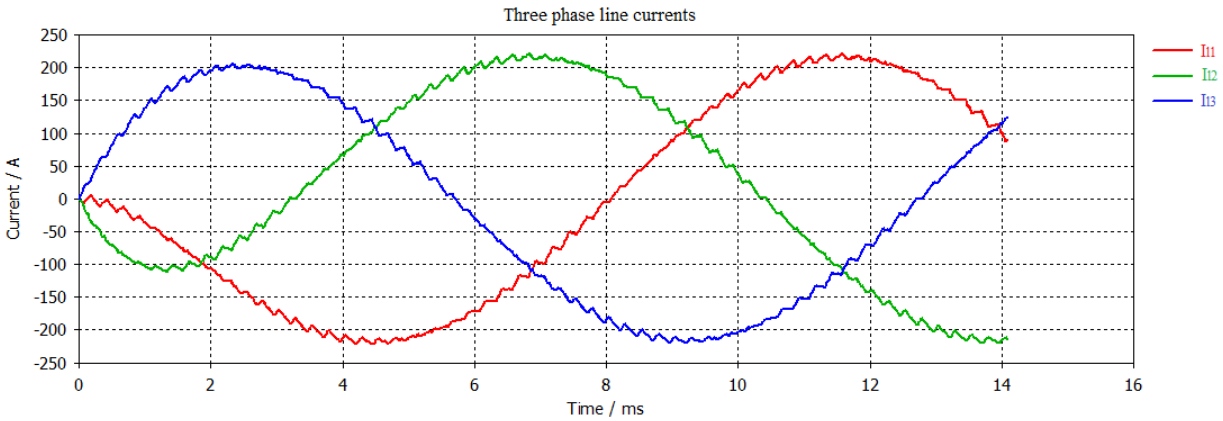

Figure 3.17. Three-phase line currents.

HF currents causing radiated emissions are decomposed in to DM and CM currents based on their mode of propagation. DM currents are high in magnitude compared with CM currents but their radiation level is relatively low due to the fact that the three lines are put close to each other enhancing natural cancellation. Moreover, DM currents mainly consist of functional three-phase currents whose fundamental component lies in LF range. CM currents, on the other hand, flow parallel with no cancellation effect. They are probable to appear in HF range since they are mainly caused by high pulsating signals. To predict the amount of radiation from the power cables, The CM current should be determined.

How CM current can be derived is well stated in [9]. CM currents running along each line are one third of the total current. The current that runs along a single phase wire, I_{cm}, is stated in Eq. 3.20 in terms of line current signals, i_a, i_b and i_c.

$$I_{cm} = \frac{i_a + i_b + i_c}{3} \tag{3.20}$$

The total current that meets at neutral point is three times this individual current,

$$I_{total,cm} = 3 \times I_{cm} = i_a + i_b + i_c$$

Simulated result of $I_{total,cm}$ is portrayed in Fig. 3.18.

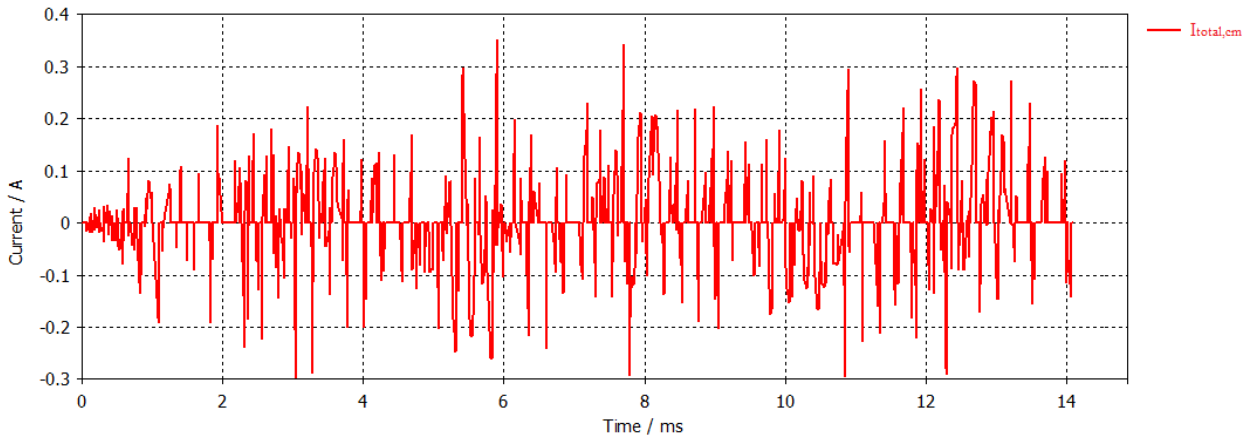

Figure 3.18. Simulated CM current in time domain.

The CM current displayed in Fig. 3.18 is the main cause of radiated emission. It results from the small ripples in the line currents (shown in Fig. 3.17). Later it is utilized as excitation input for 3D-software models. To employ that waveform for further EM simulation is, however, costly from computation perspective. The signal is nothing but just a summation of time delayed pulses

of different amplitude. Hence, by picking up the pulse with highest magnitude, it is possible to investigate the amount of radiation at that small instant. This means the time interval in which the worst radiation occurs is considered; other radiations throughout the time are equal to or less than that worst interval. Considering the highest pulse, hence, enables to investigate the severity of overall radiation level at the same time reducing simulation cost.

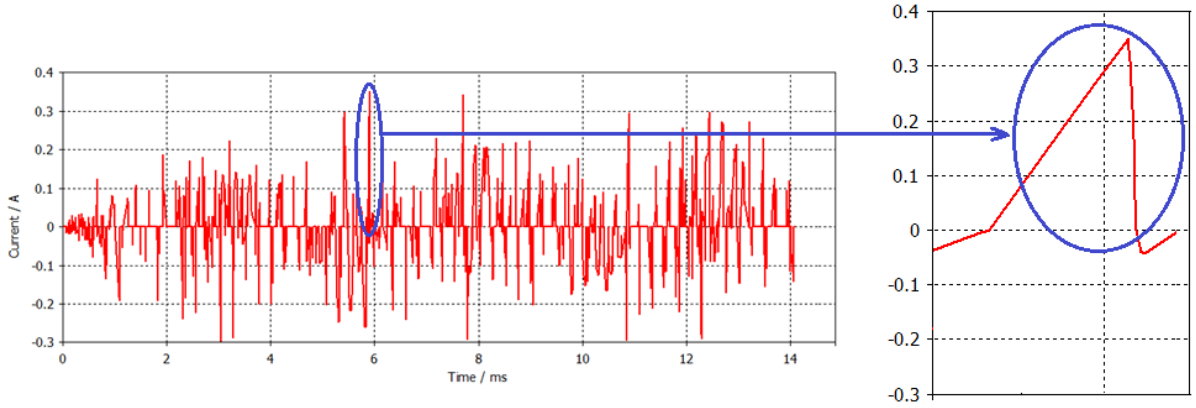

Figure 3.19. The highest current pulse in zoomed mode.

The current pulse in zoomed mode has magnitude of 0.35 A. Other pulses have relatively lower magnitude than this current pulse. Hence only the current pulse in Fig. 3.20 is used as input for further simulation. The pulse is made to advance in time in order to save simulation time.

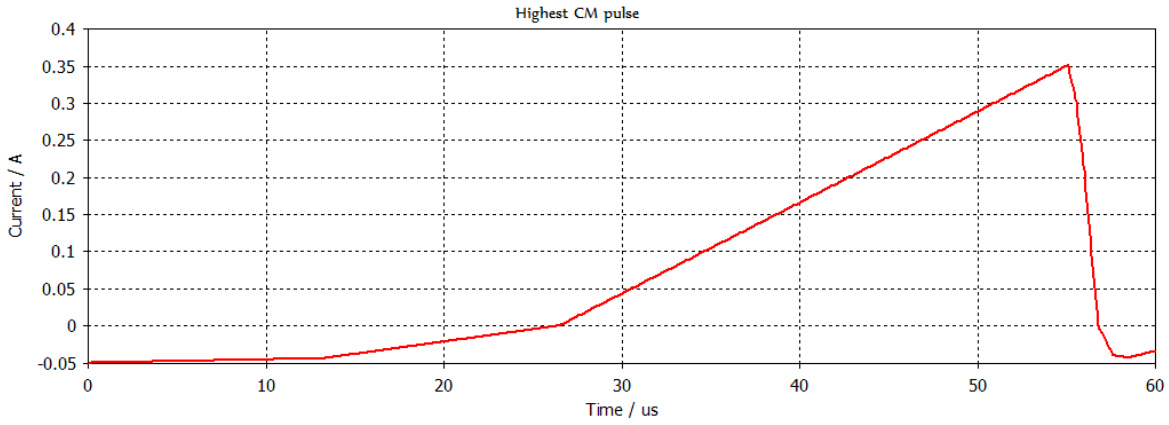

Figure 3.20. Worst pulse.

The irregular pulse in Fig. 3.20 consists of harmonic components of higher frequency. Some of the spectral contents lie in radiated emission frequency range (30 MHz - 1 GHz). Other frequency components out of this range are of no concern in this specific case.

After determining the CM current input for a structural model, configuration of more suitable circuit lay out representing the CM current as current source is required. A more simplified circuit lay out collecting the three conductors into a single conductor is depicted in Fig. 3.22. Since the three-phase lines are put close to each other, and the CM currents running along them have the same magnitude and direction, the lines can be modeled as one single conductor whose total current is just the summation of the line currents (Fig. 3.21). This current is approximately equal to the current that flows through the motor stray capacitance if small currents leaking from the transmission line through cable-shield capacitances are neglected.

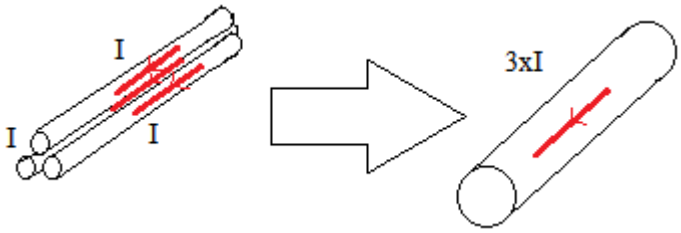

Figure 3.21. Simplification of three-phase conductors to a single conductor for CM currents analysis.

In Fig. 3.22, collected three phase lines and feeding current which is highly relevant to the current problem are modeled. With all model simplifications in mind, that model is treated as one circuit. There are four such circuits in Fig. 4.12a since four traction motors exist in a tram. The total field emission is just the summation of individual field emissions of these models.

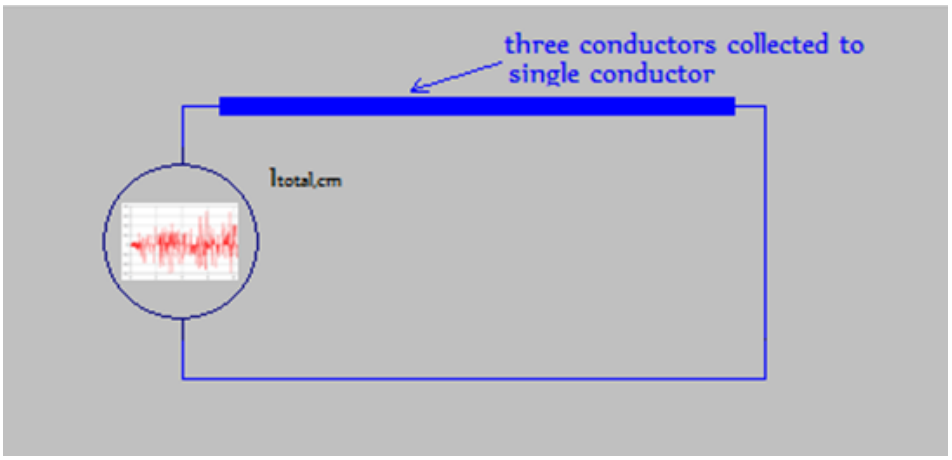

Figure 3.22. Simplified CM current source representation [Author].

All relevant information regarding RF EMF analysis has been processed to this point. What remains is final simulation of the 3D geometrical model and assessment of the result against known standards. Simulation of the model is carried out in Section 4.2.3. The final simulation is

carried out in time domain as frequency domain was not easy to handle; time-domain solver is preferred. This was simulated over a range of frequencies (30 MHz-200 MHz). Then, response of the radiative emission in that frequency range was recorded.

Chapter 4

Simulation and Analysis

4.1 Introduction

Software simulations help to ease the difficulties which would be confronted when dealing with analytical models. Moreover, analytically calculated results of complex systems are subject to errors due to inadequate modeling of the system for its complexity. Application of software is required for two purposes:

- ☞ To simulate previously developed mathematical models with range of values
- ☞ To model and simulate complex systems which are not easy to be handled analytically

Matlab is used as auxiliary simulating tool for its user-friendly interface system. LT spice software is employed as circuit simulator too. CST Studio Suite is mainly used as 3D electromagnetic simulator. Finite Integration Technique (FIT) is the simulation method employed by CST Studio Suite. Static field to HF problems are solved with spatial discretization scheme which highly features the software. To solve equations numerically, calculation domains have to be defined first. Then they are split up into many grid cells: meshing system. Tetrahedral and hexahedral meshing systems are among the widely known methods. At last, total results are calculated numerically.

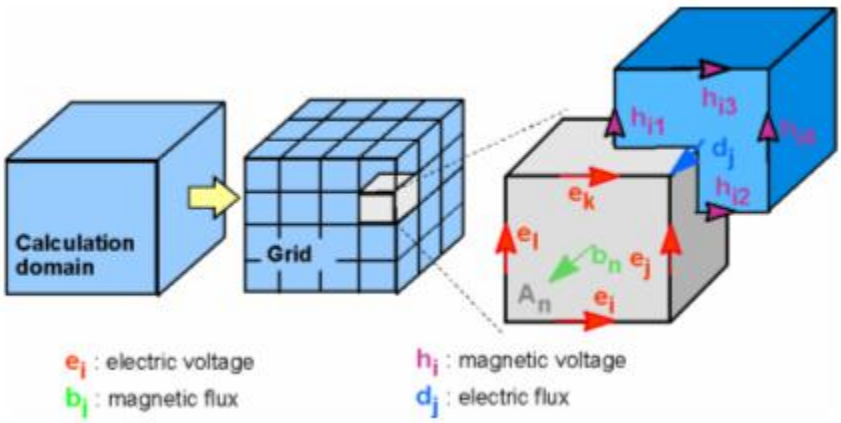

Figure 4.1. Mesh gridding system.

CST Microwave Studio, CST EM Studio and CST Cable Studio are some of the simulation modules embedded by the environment. The electromagnetic software CST EM is used for considering complex geometries, and hence, to obtain a more realistic simulation. CST EM Studio is an electromagnetic analyzer based on the FIT. It is specifically applied for the analysis and design of static and LF problems, where the wavelength is larger than the structures. CST Microwave Studio, on the other hand, is applied for HF problems.

4.2 Simulation Results

4.2.1 Simulation of Static Magnetic Fields

3D modeling of the overall system is required in order to estimate the real field pollutions inside and outside the tram. In order to simulate static magnetic fields permeating the internal and external space of the tram, determination of nearby current flows is required.

Complex structures require breaking down into manageable parts to reduce effort. Computer memory and solver times are effectively used by such method. Only relevant components of the tram, cable harnesses, are thus included in the model. The 3D model in the following figure illustrates main components of the tram which are responsible for generation of static magnetic fields. This model is derived from the 3D structure in Fig. 3.9 as discussed in the previous chapter. The dimensions of the wires inside the software are the same to the values already stated in Section 3.3.1.

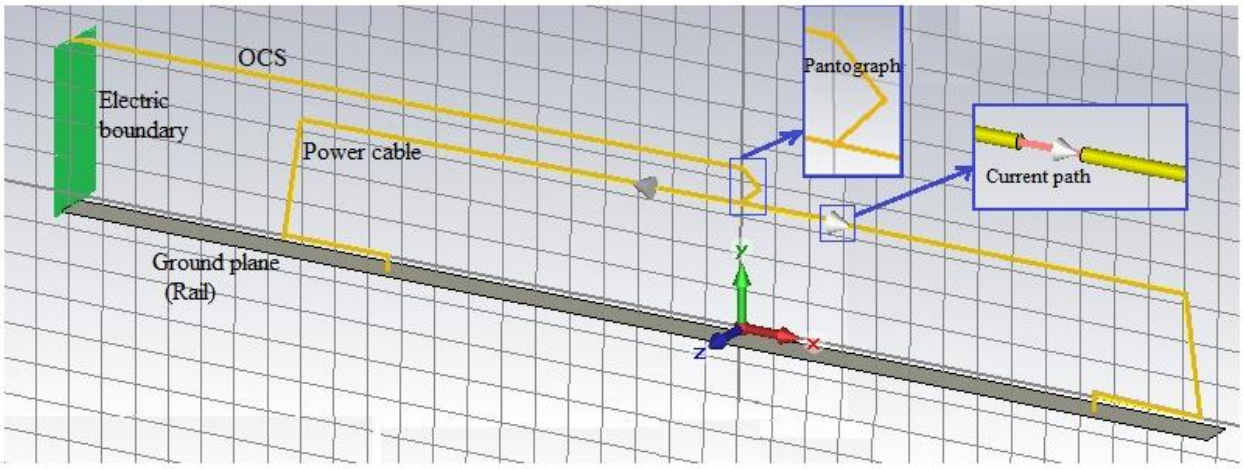

Figure 4.2. 3D model for magnetic field simulation with some zoomed in components.

For static magnetic field simulation, current paths were defined on the two symmetric sides of the tram, on the DC power cables. A current of 525 A is fed to each path. Static magnetic field was then simulated with magnetostatic solver. The 3D geometrical structure in Fig. 4.2 is run. First, field distributions around the cable harnesses were simulated and plotted as one-dimensional (1D) result along a single coordinate system. Such plotting helps to see in detail the dependence of field on a given coordinate. Then field result on two-dimensional (2D) surface was viewed. The reader should note that the coordinate system set in Fig. 3.9 (the origin of Cartesian coordinate system set at floor center of T_p car) is mainly used in the following simulations and the axes are pointing the same.

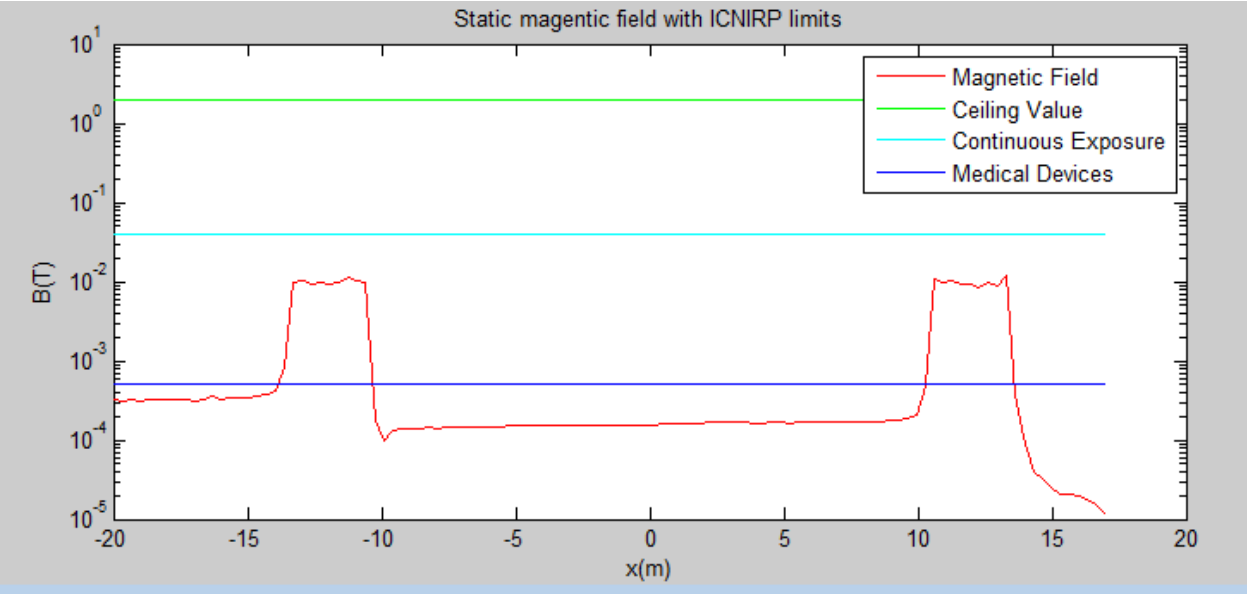

Figure 4.3. Static magnetic field distributions for $y = z = 0$, $-20 \leq x \leq 20$ with the corresponding regulatory limits.

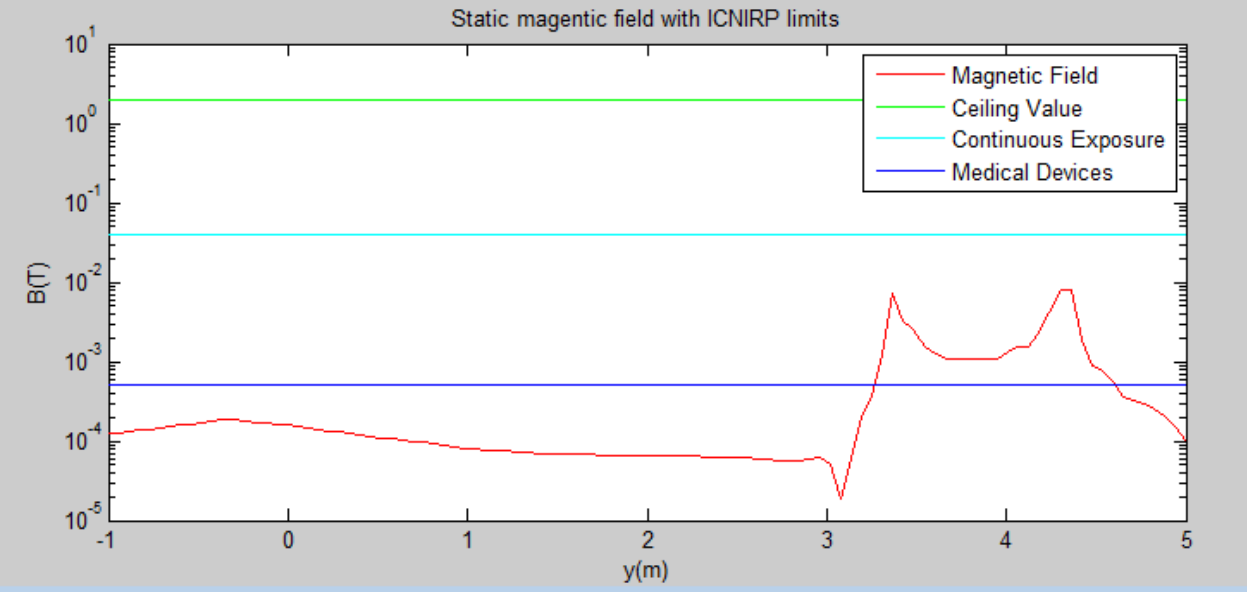

Figure 4.4. Magnetic field distributions for $x = z = 0$, $-1.5 \leq y \leq 4$ with the corresponding regulatory limits.

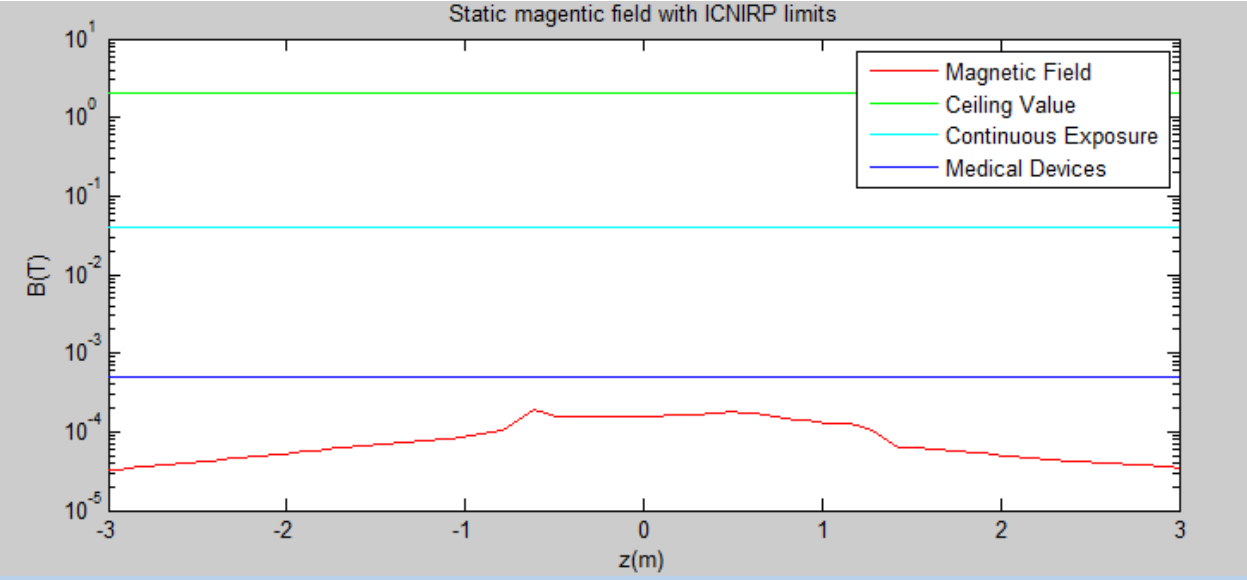

Figure 4.5. Magnetic field distributions for $x = y = 0$, $-3 \leq z \leq 3$ with the corresponding regulatory limits.

The results are plotted independently along the three axes (x, y, z) assuming the origin of Cartesian coordinate system is the same as that of Fig. 3.9. The standard exposure limits are taken from ICNIRP guidelines for static magnetic fields as illustrated in Table 2.2. The above pictures display the amount of magnetic flux density and the corresponding regulatory limits

along a given axis of the coordinate system. The following phenomena are observed from the results:

- Field distribution gets higher around the tram body than inside of it. This is due to the power cables installed on the body.
- Only exposure limit for medical devices (peacemakers) is exceeded by static magnetic fields permeating the aerial space through which DC current flows.
- The highest magnetic flux density along the y-coordinate (for $3 < y < 5$ in Fig. 4.4) is attributed to high current flow around the pantograph and OCS.

2D field distributions on a given surface give more observable results than 1D plots do. Magnetic flux density at the floor and nearby seats was determined. The choice of the floor for 2D surface field estimation helps to predict the amount of field pollution in the place where passengers are seated. The floor is around 0.36 m high from top of the rail. Simulation of magnetic field distributions in xz plane for y = 0 m is carried out. The xz plane is not specifically bounded and extends to the computation domain of the software. It can be considered as a top view of imaginary 2D surface. The structure in Fig. 4.2 was post processed for this purpose and the following 2D result was obtained.

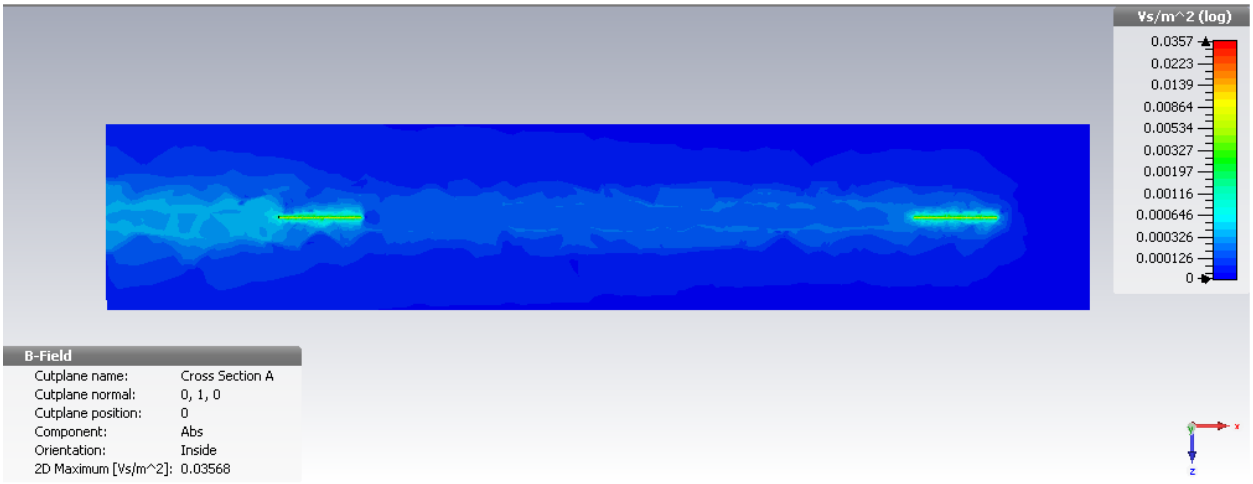

Figure 4.6. Distribution of static magnetic field in xz plane around the floor of the tram.

The 2D field distribution in Fig. 4.6 has less resolution since the color scaling extends up to the highest value. But the result still shows that the flux distribution around the floor is far below most exposure limits on static magnetic fields as previously illustrated in 1D plot results. The most probable exposure limit that is exceeded by static magnetic fields is that of sensitive

medical devices, 0.5 mT. The scaling is adjusted in order to highlight the field values exceeding that standard limit by setting the maximum value to 0.5 mT. By such a method, Fig. 4.7 clearly cuts the range of field values greater than the exposure limits for medical devices. All field values greater than 0.5 mT are equally highlighted.

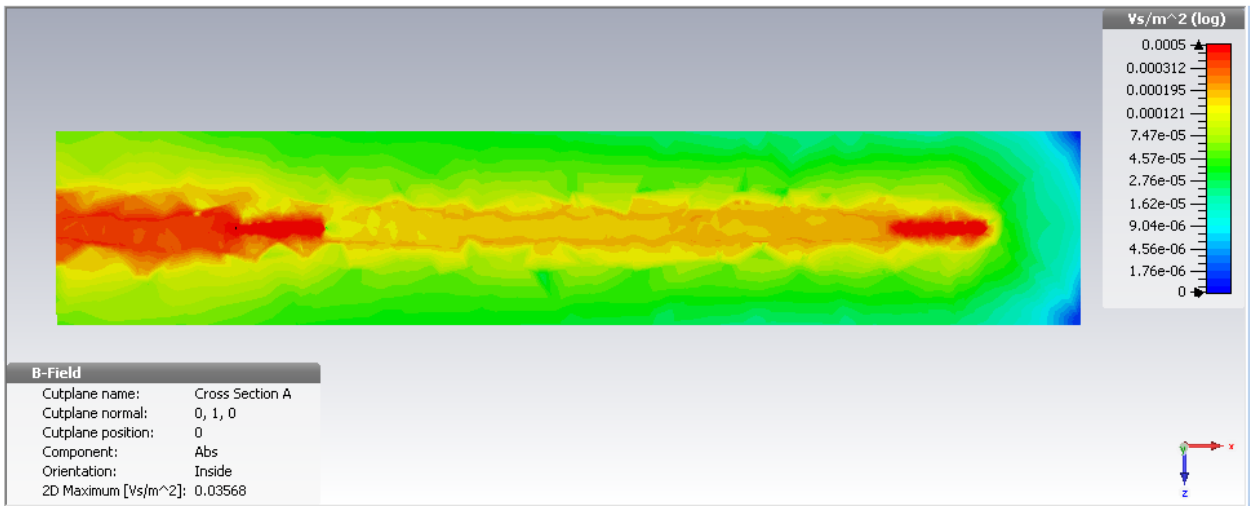

Figure 4.7. Distribution of static magnetic field in xz plane with higher resolution.

As Fig. 4.7 shows, magnetic field pollutions exceeding exposure limits for medical devices (0.5 mT) permeate around the cabs, at both ends. One end of the space is observed to have denser magnetic flux than the other. This is due to the fact that the 3D geometrical model is developed assuming the tram is fed from one side substation at a time. Also, one has to mind that all conducted simulations give more focus to the floor area. Magnetic field distributions on other locations may exhibit different nature, being weaker or denser than that of the floor area.

4.2.2 Simulation of Static Electric Fields

Electric field distribution inside the operating tram is simulated with electrostatic solver. The tram is ideally present at the point of interest, but it is excluded from the structural model as pointed out previously. The conductors shown in the figure were treated as perfect electric conductors (PEC solids) and a potential difference of 750 V was defined on them.

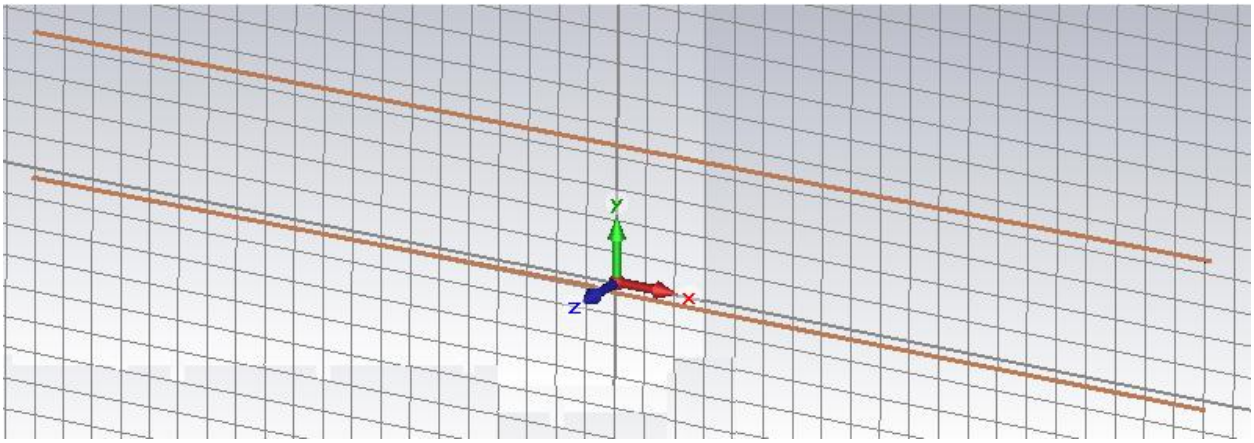

Figure 4.8. Software-developed 3D model for electric field simulation.

After the electrostatic solver is run, electric fields were observed as a result of simulation. In the following figures are 1D field distributions along single coordinate systems (y and z coordinate).

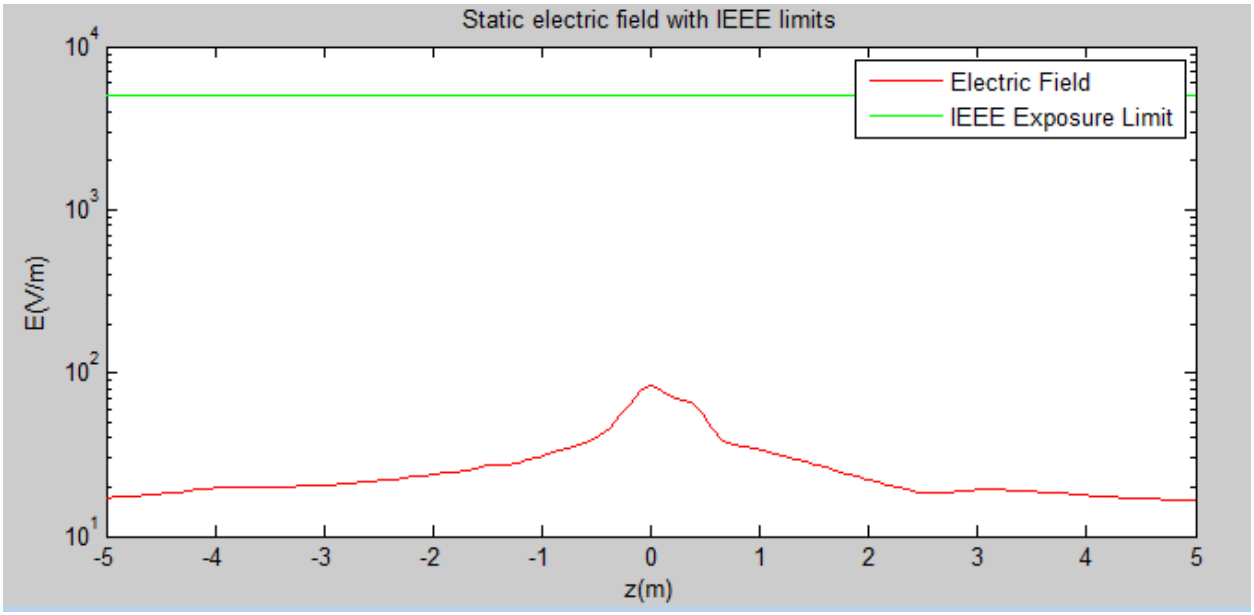

Figure 4.9. Electric field distributions for $x = y = 0$, $-5 \leq z \leq 5$.

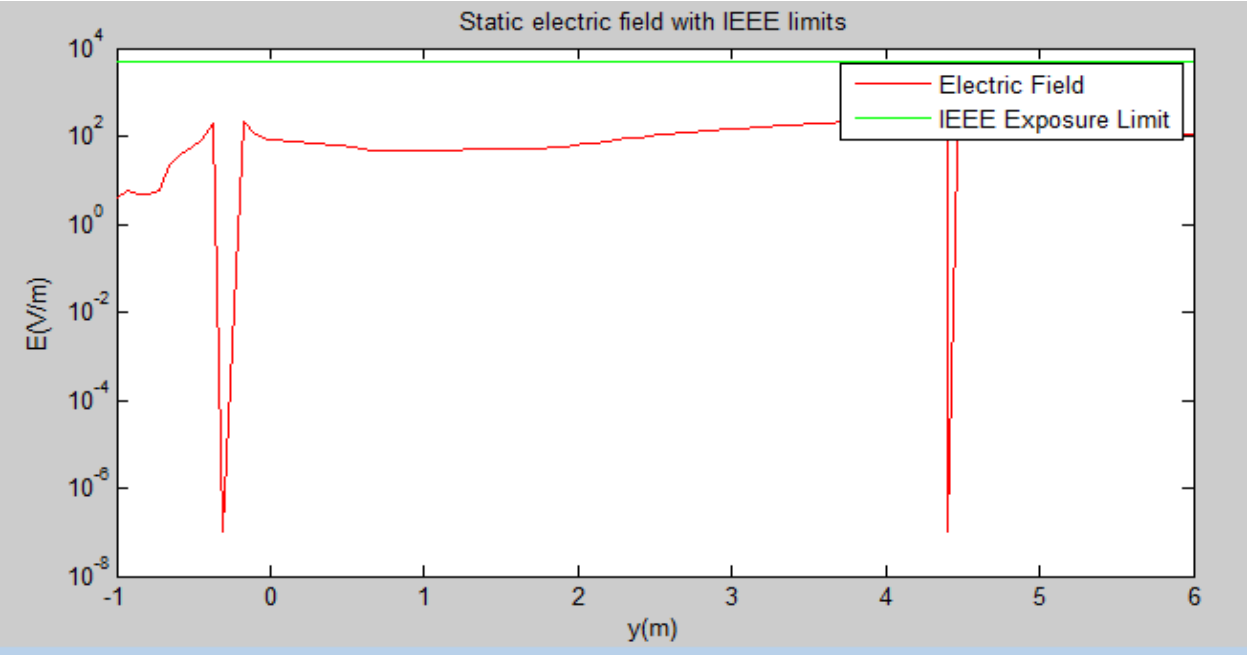

Figure 4.10. Electric field distributions for $x = z = 0$, $-1 \leq y \leq 6$.

As indicated in the graphs, electric field variation along a given coordinate system was much lower than the IEEE-set public exposure limit. Figure 4.9 shows that field strength at $z = 0$ gets highest and drops fast as the point of interest increases with z in both directions. This perfectly agrees with the inverse-distance rule.

In order to calculate field distribution around the floor (passenger compartment), simulation of electric field in xz plane for $y = 0$ (m) is carried out. In order to highlight the areas exceeding MPE limits, maximum value of the scaling is set to 5000 V/m, which is the limit value of static electric fields. 2D plot of the result is shown as follows.

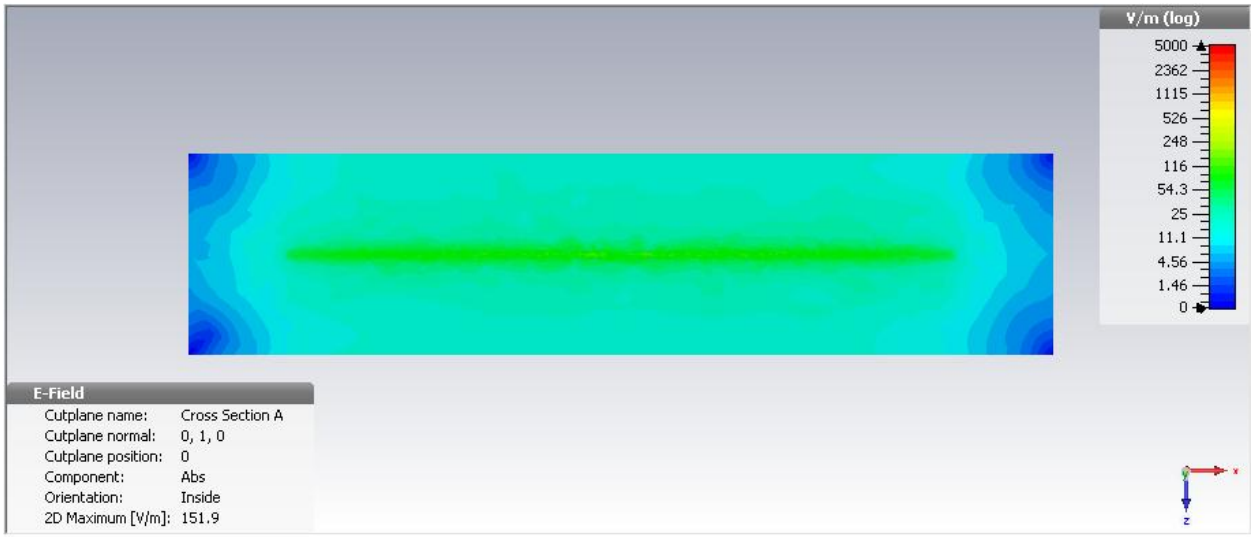

Figure 4.11. Top view of electric field distribution in xz plane around the floor of the tram.

As already observed in the single coordinate system simulations, the magnitude of electric field around the floor area is too small to exceed the exposure limits. The space surrounding OCS has relatively denser electric field than the floor area. But still the field is below the exposure limit.

4.2.3 Simulation of RF EM Radiation from Three-Phase Cables

Identification of cable geometry and representation of the CM current as current source in a schematic circuit were conducted in Chapter 3. Four schematic three-phase circuits are pictured in Fig. 4.12a. Each circuit represents the simplified circuit in Fig. 3.22. But here, it is the actual model developed inside the software; those images are direct screenshots. The number of circuits is four because there are four three-phase circuits feeding four traction motors aboard the tram. As indicated in the following figure, four external ports (numbered 1-4) are defined to each three phase circuit. Then, the sampled CM current pulse (Fig. 3.20) is made to excite each three phase circuits via those ports, and finally the simulation is done.

Because the cable model acts as a field source, uni-directional radiation is adopted as a cable field coupling type. All currents inside the cable bundle are summed up and used as a current filament in the 3D mesh. In addition to the circuit simulation, 3D field simulation which gives out the required field results is needed. This field simulation processes simultaneously with the circuit simulation because transient simulation task was preferred among others. Figure 4.12b

illustrates a structural model for field simulation. This model is developed in 3D domain and represents the positioning of three-phase power circuits installed aboard AA LRT tram. It is in-software-built version of the one shown in Fig. 3.13 and hence its dimensions are set the same.

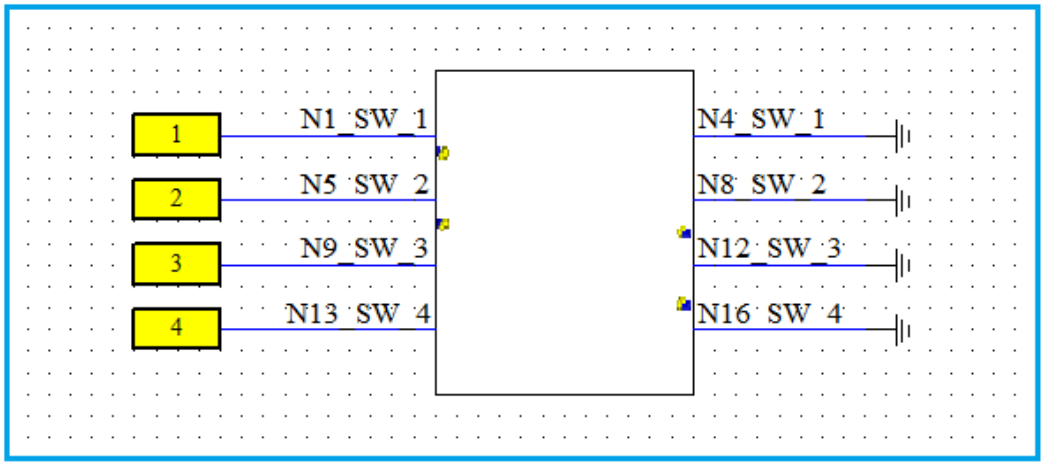

(a)

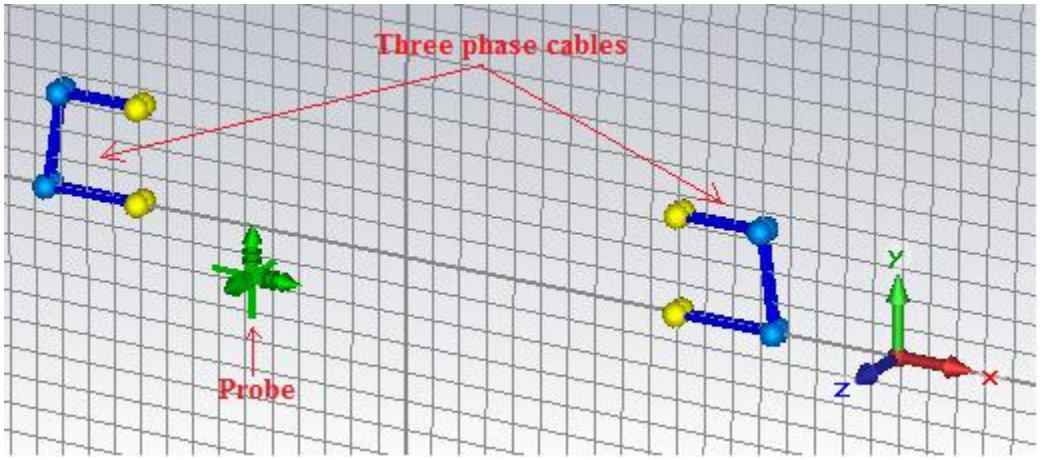

(b)

Figure 4.12. Simulation layout. (a) Schematic model. (b) 3D model with probe.

After the current spike in Fig. 3.20 is fed to the schematic circuit, 3D EMF simulation simultaneously runs for far field region. In fact, the frequency range in which radiated emission are measured is 30 MHz up to over 1 GHz. But here, the range was truncated to 30 MHz - 200 MHz because the spectral contents beyond 200 MHz are very small in magnitude and their impact is almost insignificant. For combined RF EM waves, electric field is usually taken as a limiting parameter. Hence at a given distance from the field source, electric field strength which

would be applied for assessment purpose is recorded. As shown in Fig. 4.12b, a probe was located at 10 m distance and 3 m height, as per the FCC regulation for radiated emissions.

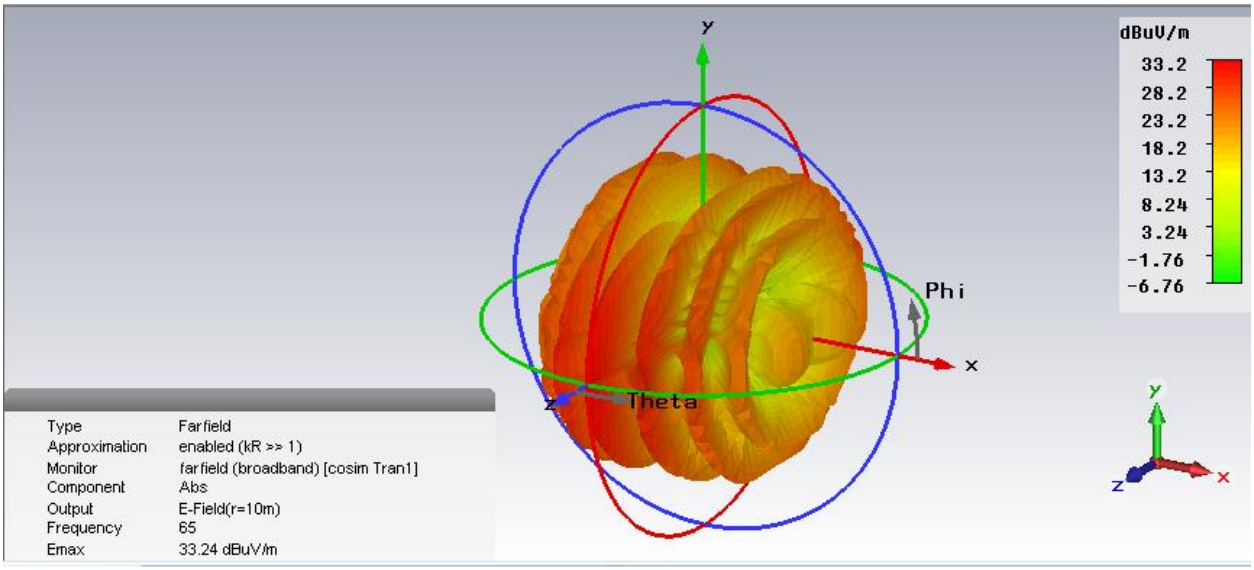

Figure 4.13. Total field value at probe location.

Figure 4.13 illustrates single frequency absolute value of the total electric field that permeates at the measuring point, the place where measurement antenna is placed. In software simulations, probes replace the work of antenna. The radiated emissions are measured with the measurement antenna in both the vertical and horizontal polarizations with respect to the ground plane. The product's field must not exceed the regulatory limits in both polarizations. Cartesian coordinate system attached to the measuring probe is used for estimating fields in both vertical and horizontal polarization. The xz plane is thought as the ground plane. Hence the x axis, which is parallel to the plane, represents horizontally polarized antenna whereas the y axis, which is perpendicular to the plane, represents vertically polarized antenna. Assuming net radio wave energy travels toward the probe from the origin of Cartesian coordinate system, the electric field in both horizontal and vertical polarizations is recorded. Resultant electric fields as function of frequency are displayed in the following figures together with FCC regulatory limits for Class A devices.

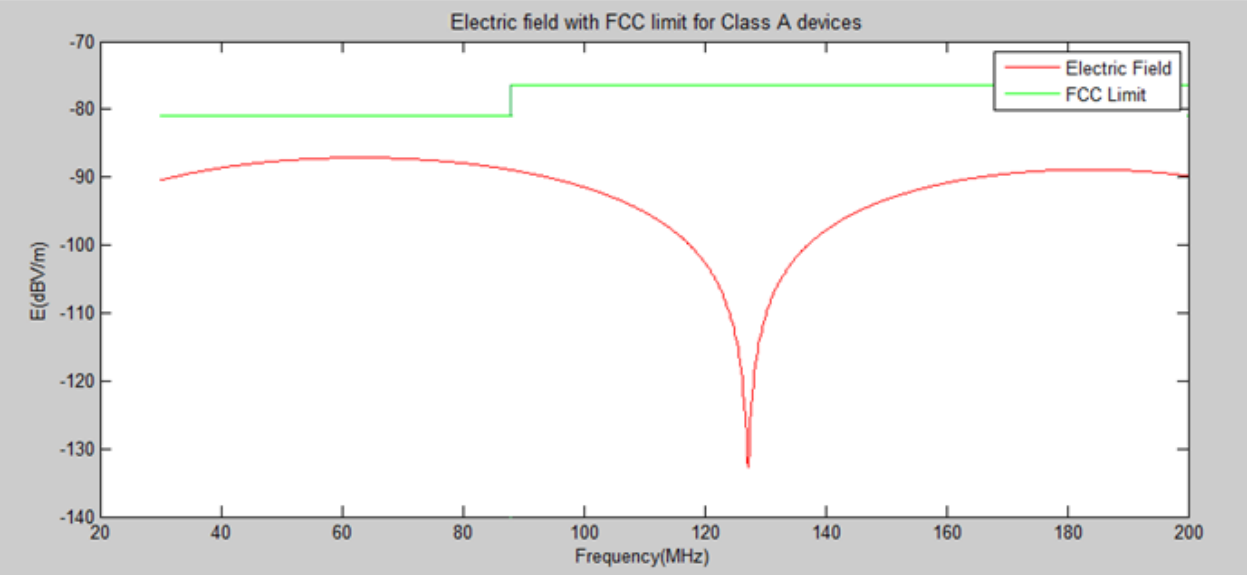

Figure 4.14. Electric field emission in vertical polarization.

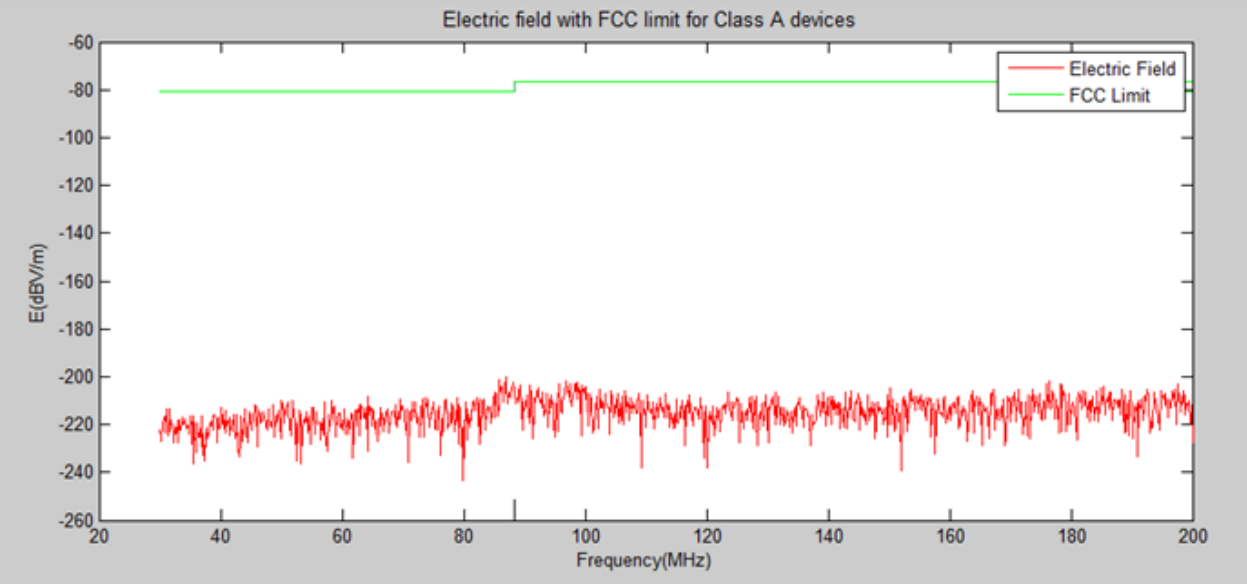

Figure 4.15. Electric field emission in horizontal polarization.

All the above results show that electric field strength in vertical polarization is higher than the field strength in horizontal polarization. Still, RF EM radiation in both polarizations was below the regulatory limit. Because they mainly belong to industrial applications, onboard LRT equipments were treated as Class A devices. If they were assumed as Class B devices, however, the result would change showing some violations in certain frequency ranges.

Chapter 5

Conclusion, Recommendation and Future Work

5.1 Conclusion

In this thesis, EM radiation from on-board cable harnesses has been studied. Software was mainly used to compute both LF and HF field distributions inside and outside the LRT tram. In order to obtain field emission of the real system, all physical and electrical parameters representing the real LRT system were used in software model. An origin of Cartesian coordinate system was set on the floor, at the bottom center of the T_p car. Static electric field and static magnetic field distributions along the three coordinates were computed. This helps to observe how the field density varies as function of distance from inside the tram. 2D field distribution around the floor of the locomotive was also computed. The reason why the floor area was selected for 2D simulation is that it is mainly occupied by passengers along with their baggage which are going to be the victim of EMI. As a result, estimation of EM pollution around the floor area was important. For RFI computation, a probe was set at 10 m distance and 3 m height. Sample of CM current spike responsible for RF emission was selected and fed to previously developed 3D model in order to estimate the existing EM noise.

LF and HF EM pollutions had their respective standard limits to compare with. All simulated results were assessed against those standard regulatory limits. Based on the results and findings, it was possible to draw the following conclusions.

- Static magnetic field which exceeded regulatory limit for medical devices (0.5 mT) was observed around the driver's cab and near the interface between pantograph and OCS. The space where such phenomenon was observed is, however, limited. It dramatically drops as the point of measurement moves outward the tram body. Exposure limits other than that for medical devices were never exceeded in the internal space of the tram. Medical infrastructures implanted at ≥ 3 m distance on-side the track are rarely affected by static magnetic fields emanating from LRT tram.

- MPE limit on static electric field is 5 kV/m. Even the highest voltage difference (DC 750 V between OCS and ground) doesn't cause static electric field emission which approaches the regulatory limit. Hence the system does not generate static electric field problems.
- The other point deduced from the result is that harmonic nature of the inverter-output voltage leads to generation of CM current circulating through the stray capacitances. Radiations caused by CM current are directly related to the length of the structure, not to its loop area. In RFI study, transient simulation of 3D model with CM current spike as input was conducted. Still, the electric field emissions in both the vertical and horizontal polarizations were below the regulatory limit. The model was developed assuming no mitigation techniques (like filters) are employed to the inverter-motor path. If these defense mechanisms are already applied, radiation emission from that specific area would be reduced further.
- Other sources of RFI such as radio communication systems and ambient electrical systems were not included in the model. But in reality, the field emission is cumulative result of individual RF emissions from different systems present in the site. This is what makes EMI prediction more challenging, varying from time to time and place to place even for the same product under test.

Generally, field emissions from cable harnesses on board LRT tram were below the standard regulatory limits. In some points, it was observed that static magnetic field density exceeded the regulatory limit for medical devices. But the area where such phenomenon was observed was around the tram body. There is less probability of sensitive electromedical devices approaching that area.

5.2 Recommendation

In the conclusion part, it was shown that most of simulation results were generally below the standard regulatory limits. But it should also be noted that they were the outcome of a single scenario, and EMI result depends on many internal and external circumstances. Hence all potential hazards should be lessened by employing extra measures.

Amount of EM radiation from a given device depends on how wide the planar structure or how long the linear conductor is. It is recommended that onboard interconnecting cables of LRT trams (especially those carrying HF harmonics) should have as minimum length as possible. The traction inverters of AA LRT are placed on the roof of the tram, whereas the driven motors are placed on the floor; three-phase interconnecting cables pass down through the tram body, covering a large distance. If the inverters are placed on the floor of the tram, the distance between inverter and motor greatly reduces implying less EMI potential.

Another issue that should be of great concern is the usage of mitigation techniques. In fact, it was not possible to see whether the inverter-motor path was equipped with EMI suppressing circuits because the motor was already packaged. If no mitigation techniques are employed previously, they should be considered in future design. One efficient method of avoiding HF harmonics is the usage of a low pass filter inserted between inverter and motor.

5.3 Future Work

Simulation results in this thesis are based on many assumptions. The developed models may not parallel the real on-board systems from stand point of accuracy. Therefore, practical measurement of EMI on board LRT trams is required in order to obtain more accurate results. Also, a study considering the effect of more than one trams on parallel tracks should be conducted in order to get more realistic results.

Reference

[1] C. R. Paul. *Introduction to Electromagnetic Compatibility*, 2nd ed. New Jersey, United States: John Wiley & Sons, 2006.

[2] R. J. Hill. Electric Railway Traction 6. Electromagnetic Compatibility-disturbance sources and equipment susceptibility. *Power Engineering journal*, Feb 1997, vol.11

[3] J. Ben Hadj Slama, D. Chariag. Measurement and Analysis of Magnetic Field Radiation from D.C Tramway: A case study for Tunis's metro. *Journal of Electrical Systems*, 1-12, 2008.

[4] EMI/RFI Generation from Light Rail Transit Systems. *Electric Research and Management, INC*, April 2013

[5] DIB Djalel, MORDJAOUI Mourad. Study of the influence high-voltage power lines on environment and human health (case study: The electromagnetic pollution in Tebessa city, Algeria). *Journal of Electrical and Electronic Engineering*, 2(1):1-8, February 2014. 10.11648/j.jeee.20140201.11

[6] Ioan TILEA, Calin MUNTEANU. Study of electromagnetic interference in inverter driven asynchronous motors. 695-700, 2012

[7] Sabine Marksell. *EMC Aspects of PWM Controlled Loads in Vehicles.* Lincentiate Thesis. Lund University ; 2004.

[8] S. Schulze, M. Al-Hamid, R. Vick, and R. Doebbelin. Modeling the Electromagnetic Behavior of Power Converters. *Progres in Electromagnetics Research Symposium Proceedings.* 449-453, Cambridge, USA: July 2010.

[9] Gabriele Grandi, Domenico Casadei, Ugo Reggiani. Analysis of Common-and Differential-Mode HF Current Components in PWM Inverter-Fed AC Motors.

[10] V.Deniau, N. Ben Slimen, S. Baranowski, H.Ouaddi, J.Rioult and N.Dubalen. Characterization of the EM Disturbances Affecting the Safety of the Railway Communication Systems. *The European Physical Journal Applied Physics*, 43(2):225-250, August 2008. 10.1051/epjap:2008053

[11] IEC61000: Electromagnetic compatibility, 2000.

[12] *Drive Engineering-Practical Implementation-EMC in Drive Engineering*

[13] http://hps.org/hpspublications/articles/elfinfosheet.html

[14] World Health Organization, International Agency for Research on Cancer. Non-ionizing radiation, Part 1: Static and extremely low-frequency (ELF) electric and magnetic fields Exit Disclaimer. *IARC Monographs on the Evaluation of Carcinogenic Risks to Humans* 2002; 80:1-395.

[15] Institute of Electrical and Electronics Engineers (IEEE). IEEE PC95.6-2002. *Standard for safety levels with respect to human exposure to electromagnetic fields, 0 to 3 kHz.* Prepared by Subcommittee III of Standards Coordinating Committee 28, IEEE Standards Department. New York: Institute of Electrical and Electronics Engineers, Inc.; 2002.

[16] European Union Council*: Recommendation of 12 July 1999 on the limitation of exposure of the general public to electromagnetic fields (0Hz – 300GHz), (1999/519/EC).*

[17] ICNIRP Guidelines. *Guidelines on limits of exposure to static magnetic fields.*

[18] C. R. Paul and S. A. Nasar. *Introduction to Electromagnetic Fields,* 2nd ed. McGraw- Hill, New York, 1987.

[19] East-West Line (Phase I) Project of Addis Ababa, Ethiopia, *Technical Specifications of Vehicles*.

[20] Tsegu Worku. *Analysis of Electromagnetic Emission from Contact lines of Light Rail Transit System.* MSc Thesis. Addis Ababa University; July 2014.

[21] Demissu Legese. *Harmonic Analysis of Addis Ababa Light Rail Transit Traction Converters.* MSc Thesis. Addis Ababa University; August 2014.

Appendix A

Motor Parameter Calculation

According to AA LRT data, the active power of a motor is 130 kW whereas the reactive power is 63 kVAr. Apparent power is derived from the given power factor, *pf* as follows.

$$S = \frac{P}{pf}$$

$$= \frac{130\ kW}{0.9} = 144.44\ kVA \tag{A.1}$$

In order to estimate impedance of each phase winding, knowledge of rms phase voltage and power is required. Each of the three phases contributes 1/3 of the total power.

$$S_{ph} = \frac{144.44\ kVA}{3} = 48.1\ kVA$$

$$P_{ph} = \frac{130\ kW}{3} = 43.3\ kW$$

$$Q_{ph} = \frac{63\ kVAr}{3} = 21\ kVAr$$

The phase voltages have a value of V_{ph} = 288.5 V. Total impedance of each phase winding is thus found after some steps.

$$I = \frac{S}{V}$$

$$= \frac{48.1\ kVA}{288.5\ V} = 166.7\ A \tag{A.2}$$

I is the rms line current. Maximum rated line currents can reach 210 A as stated in [19]. The three power forms (apparent, active and reactive) can be expressed in terms of the rms line current as:

$$S = I^2 Z$$

$$P = I^2 R$$

$$Q = I^2 X$$

The powers and current are known. The real and imaginary impedances of the phase winding can thus be simply evaluated from the above equations.

$$Z = \frac{S}{I^2}$$

$$= \frac{48.1\ kVA}{166.7^2\ A^2} = 1.731\ \Omega \quad \text{(A.3)}$$

$$R = \frac{P}{I^2}$$

$$= \frac{43.3\ kVA}{166.7^2\ A^2} = 1.56\ \Omega \quad \text{(A.4)}$$

$$X = \frac{Q}{I^2}$$

$$= \frac{21\ kVAr}{166.7^2\ A^2} = 0.755\ \Omega \quad \text{(A.5)}$$

The impedance Z = 1.56 Ω + j 0.755 Ω can be modeled as a series resistor and inductor of each of the motor windings. 1.56 Ω represents the real impedance of the winding, the resistor. The imaginary impedance, 0.755 Ω, is that of the inductor connected in series with the resistor. After all these steps, the inductance value can be calculated based on the following formula.

$$L = \frac{X}{2\pi f}$$

$$= \frac{0.755\ \Omega}{2 \times \pi \times 71\ Hz} = 1.69\ mH \quad \text{(A.6)}$$